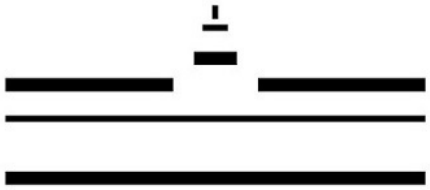

Characterisation of a photocathode for a monoenergetic electron source for the KATRIN experiment

Bachelor thesis

Raffaela Busse

Westfälische Wilhelms-Universität Münster
Institut für Kernphysik
AG Prof. Dr. C. Weinheimer

2014

Referent: Prof. Dr. C. Weinheimer
Korreferent: PD Dr. C. Klein-Bösing

Contents

1 Introduction **1**
- 1.1 Neutrinos and KATRIN . . . 1
  - 1.1.1 The KATRIN setup . . . 2
  - 1.1.2 MAC-E filter technique and transmission function . . . 3
- 1.2 Motivation of this bachelor thesis and contribution to the KATRIN experiment . 5

2 Theoretical foundations and technical devices **6**
- 2.1 The photoelectric effect . . . 6
- 2.2 Semiconductors and p-n junction . . . 6
  - 2.2.1 LEDs . . . 7
  - 2.2.2 Photodiodes . . . 7
- 2.3 Monochromator . . . 7
- 2.4 Work function . . . 8
  - 2.4.1 Coherence of work function and wavelength . . . 9
- 2.5 Measuring errors . . . 10

3 The experimental setup **11**
- 3.1 The test setup . . . 11
  - 3.1.1 Light sources . . . 11
- 3.2 The angular selective electron gun (eGun) . . . 15
  - 3.2.1 The energy spectrum of the eGun electrons . . . 16

4 Calibration of the setup components **18**
- 4.1 Monochromator calibration . . . 18
  - 4.1.1 Calibration by means of the laser . . . 18
  - 4.1.2 Calibration by means of the UV LEDs . . . 19

5 Characterisation of the eGun-photocathode **21**
- 5.1 Long-term measurements . . . 21
- 5.2 Work function measurements . . . 25

6 Summary and Outlook **28**

7 Appendix **30**

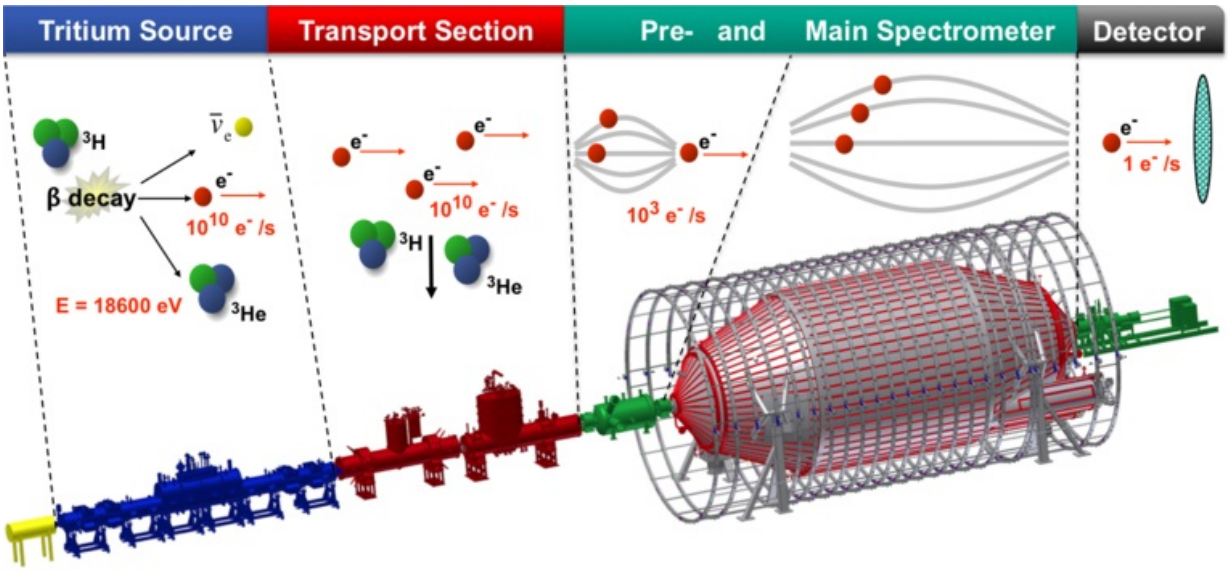

Figure 1: **Setup of the KATRIN experiment.** The setup sections most relevant for this bachelor thesis are the Pre- and Main Spectrometer as described in section 1.2. [KIT13]

1 Introduction

1.1 Neutrinos and KATRIN

Ever since their discovery, neutrinos have been a mystery to scientists all over the planet. Because they are only affected by weak interaction – they neither carry electric nor colour charge – it has been really difficult to detect them or, let alone, to examine their properties. Physicists first thought of these very light, neutral particles when they analysed the energy spectrum of the beta decay and saw that it was continuous. That meant there had to be another particle besides the daughter nucleon and the beta particle that has not been detected ever before. So Pauli postulated the neutrino in 1930 as a neutral, massless particle.
Nowadays, neutrinos are considered massive and form an inherent part of the Standard Model of particle physics. In fact, they are the most abundant massive elementary particles in our universe what makes them an important object of research.

By means of the *Karlsruhe-Tritium-Neutrino-Experiment* (KATRIN), which is shown in fig. 1, the mass of the anti electron neutrino $\bar{\nu}_e$ is to be determined by measuring the tritium beta decay (^3H β-decay) energy spectrum very accurately. The endpoint of the energy spectrum can give information about the neutrino mass.

The beta decay has two decay products, the electron and the anti electron neutrino. So the energy that gets released during the decay is split in any way between these two particles. Now imagine the electron gets *all* the kinetic energy – then, if the anti-electron neutrino is

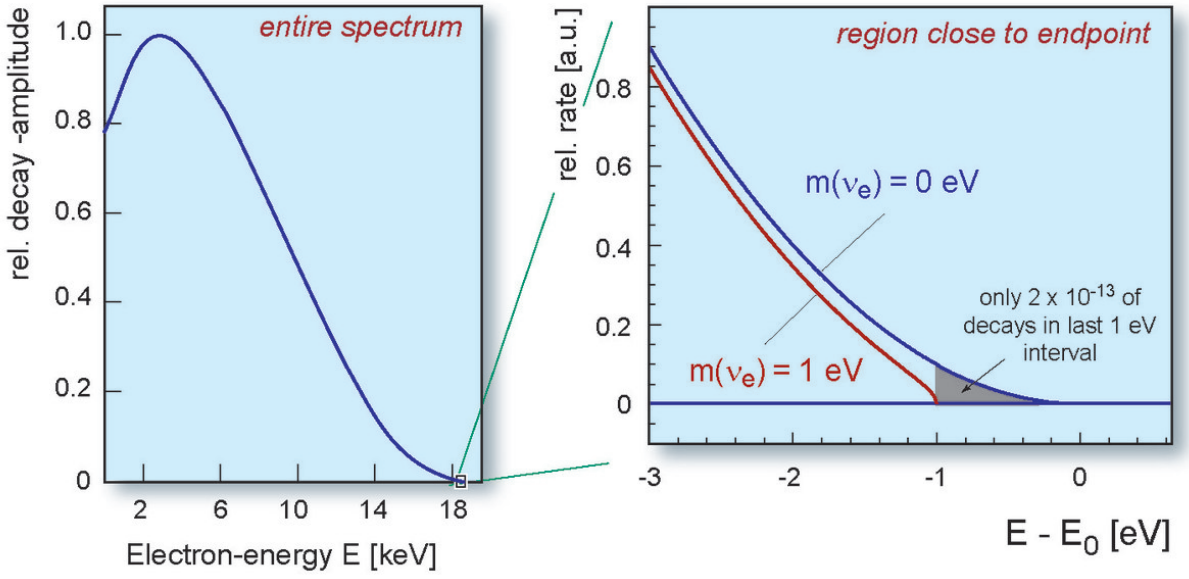

Figure 2: Energy spectrum of the tritium β-decay. [KIT13]

massive[1], it has to keep at least its own rest energy which is exactly what KATRIN is looking for. The difference between the theoretical endpoint of the spectrum for massless neutrinos and the actual endpoint measured by KATRIN accords to the anti-electron neutrino mass. Fig. 2 shows the endpoint of the spectrum with the blue curve for massless neutrinos and the red curve implying an exemplary neutrino mass of $m_{\bar{\nu}_e} = 1\,\text{eV}$.

The experimental setup of KATRIN is described in the following passage.

1.1.1 The KATRIN setup

In fig. 1 the over 70 m long setup of the KATRIN experiment at the KIT in Karlsruhe is shown. The blue setup section shows the **tritium source** of the KATRIN experiment. Here the anti electron neutrinos and the beta electrons are generated via the β^--decay of tritium. These electrons have got energies up to $E_{\beta,max} = 18,6\,\text{keV}$. In the following **transport section** (red), the electrons are passed on to the pre-spectrometer while the radioactive decay products ^3H and ^3He are filtered out. The neutrinos escape the source undetected.
The **pre-spectrometer** (green) can be seen as a smaller version of the main spectrometer and works as an MAC-E filter (see section 1.1.2). Here, unwanted low-energy electrons get reflected to reduce the total electron flux that enters the main spectrometer to $\approx 10^3\,\text{s}^{-1}$.

[1]The neutrino mass is a consequence of the theory of neutrino oscillation. This theory involves different mass eigenstates that mix into different neutrino flavours (electron, myon and tau neutrino).

The **main spectrometer** (green) is the heart of the KATRIN experiment. It is a MAC-E filter like the pre-spectrometer, but with much higher resolution due to its larger dimensions. The vessel consists of a vacuum tank with a length of over 23 m and a diameter of 9.8 m made of stainless steel. The tank provides the retarding potential. The inner surface is covered with a complex structure of wire electrodes with which the retarding potential can be fine-tuned. The electrodes also shield the flux tube from secondary electrons created by cosmic muons or radioactive decays in the vessel walls. The magnetic field inside the vessels is provided by superconducting solenoids at the entrance and the exit ($\approx 4,5$ and 6 T) of the spectrometer. The air coil system surroundig the vessel corrects for the Earth's magnetic field and allows to fine-tune the magnetic field inside the spectrometer. By means of the MAC-E filter technique, an integrated energy spectrum of the tritium beta decay electrons can be measured by varying the electric retarding potential at the analysing plane and taking the electron count rate (which depends on the retarding potential, order $< 1\,\mathrm{s}^{-1}$) at the detector. The **detector** consists of a PIN diode with 148 segmentations which allows a spatial discrimination of the counted electrons. [Beh12]

1.1.2 MAC-E filter technique and transmission function

The MAC-E filter technique is applied in both the pre- and main spectrometer of the KATRIN experiment and is exemplified by means of the main spectrometer filter which is shown in fig. 3. This type of filter consists of two essential elements: a magnetic field at the one hand and a retarding electric potential at the other.

The magnetic field inside the main spectrometer is generated by two superconducting solenoid magnets both at the entrance and the exit of the vessel. The maximum magnetic field strength B_{max} is achieved right inside the solenoids whereas the minimum field strength B_{min} is located in the middle of the vessel at the so-called analysing plane. At this plane, the retarding electric potential, generated by the wire electrodes inside the spectrometer, reaches its maximum value U_0.
An electron entering the spectrometer undergoes adiabatic cyclotron motion along a magnetic field line, so its kinetic energy has a transversal and a longitudinal part. Hence to the adiabatic movement, the magnetic flux remains constant which leads to an almost entirely transformation of its transversal energy into longitudinal energy when reaching the analysing plane:

$$E_{\perp} \rightarrow E_{\parallel} \tag{1}$$

Here, the electric and magnetic field lines are parallel, so only electrons with a sufficient longitudinal energy (the transversal energy is irrelevant to the retarding potential) can pass the analysing plane and are transmitted to the detector; electrons with lower longitudinal energies get reflected. The longitudinal energy at the analysing plane depends on the starting angle of the electron relative to the magnetic field line. Electrons with fixed kinetic energy but different starting angles will have different longitudinal energies at the analysing plane. This dependency of the electron transmission probability on the starting angle is the main

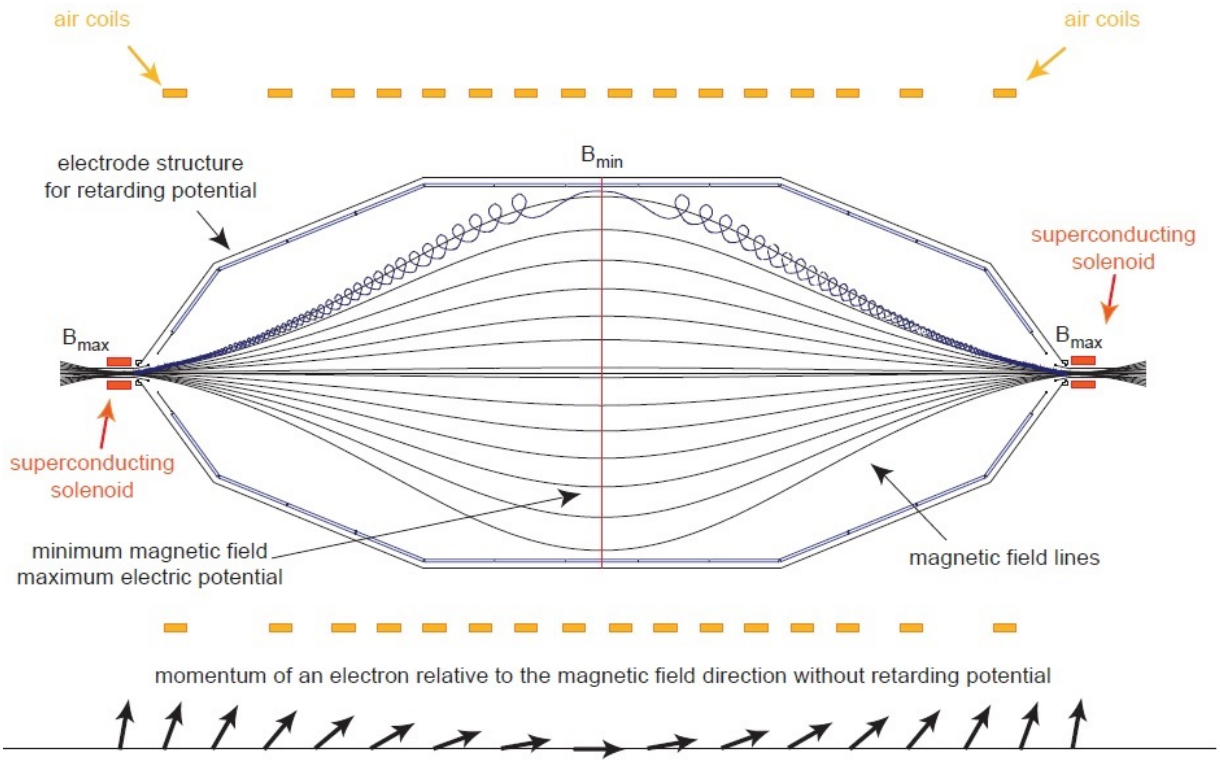

Figure 3: **The KATRIN main spectrometer MAC-E filter (schematically).** Shown is the vessel with the surrounding air coils (yellow), the wire electrode structure (blue), the solenoids at both ends (red) and the magnetic field lines inside (black). The adiabatic movement of an electron is drawn along the top magnetic field line (blue). At the bottom of the figure the changing momentum of an electrom moving inside the spectrometer is shown [Hug08].

reason for the angular selective electron gun which this bachelor thesis is about. The electron gun allows to characterise the transmission properties of the main spectrometer; more on that in section 1.2.

The energy resolution of an MAC-E filter depends on the ratio of B_{max} and B_{min} and therefore on the spectrometer size:

$$\Delta E = E_{\mathrm{start}}^{\mathrm{max}} \cdot \frac{B_{\mathrm{min}}}{B_{\mathrm{max}}} = 0.93\,\mathrm{eV}\,, \tag{2}$$

with $B_{\mathrm{max}} = 6\,\mathrm{T}$ inside the solenoids and $B_{\mathrm{min}} = 3 \cdot 10^{-4}\,\mathrm{T}$ at the analysing plane; $E_{\mathrm{start}}^{\mathrm{max}} = 18.6\,\mathrm{keV}$ is given by the endpoint of the tritium beta decay spectrum. [Beh12]

1.2 Motivation of this bachelor thesis and contribution to the KATRIN experiment

As mentioned above, the transmission of the electrons in the KATRIN main spectrometer depends on their starting angle relative to the magnetic field lines. Electrons with different starting angles hit different segmentations of the detector, which leads to different transmission functions for each of the 148 detector pixels due to the inhomogenities in the electromagnetic field. These transmission functions have to be determined so that variances in the electric potential can be located and compensated for later measurements. Since the tritium source emits electrons with random starting angles it is not suitable for this kind of spectrometer calibration. So the *Institut für Kernphysik* at the WWU Münster built an angular selective electron gun (eGun) which will be installed at the front opening of the main spectrometer. By means of its angular selectivity, electrons moving along any possible magnetic field line with any desired starting angle can be analysed.

The eGun emits photoelectrons that are ejected from a thin gold layer (in previous measurements: silver layer) as a photocathode via the photoelectric effect. The layer is evaporated to the optical fibre at the CeNTech in Münster. The photoelectrons have to be monoenergetic to calibrate the spectrometer as accurately as possible. This is realised by choosing an ultraviolet (UV) light source that emits photons with energies near the work function of the gold layer, so that the electrons ideally have no kinetic energy when leaving the layer surface[2]. Afterwards, they can be accelerated to the desired energy in an electric field.

The gold photocathode has to be characterised to find its specific work function[3] and therefore the ideal photon wavelength to eject zero-energy electrons. By taking the count rate of ejected electrons for different photon wavelengths the work function can be determined. The photons can be generated either by a pulsed laser with a defined wavelength or by UV-LEDs with different wavelengths in the UV range. To find the work function and to test the gold photocathode for its long-term stability is the subject of this bachelor thesis.
For that purpose the existing hard- and software [Pot13] has to be upgraded and revised. Also, the hardware has to be calibrated and integrated in the eGun setup before first test measurements can be performed.

[2]The work function is the minimum energy needed to eject electrons from a surface. If the photon energy exactly equates the work function, the ejected electrons have no surplus kinetic energy. This is very difficult to realise because of impurities of the layer etc., but the surplus kinetic energy can be approximately kept to a minimum.

[3]The specific work function differs from the theoretical work function of gold because of impurities or depositions on the layer that can not be completely prevented. Other important effects that influence the specific work function are explained in [Win14].

2 Theoretical foundations and technical devices

This section provides the theoretical basis necessary to understand the physical processes concerning the experiments with the eGun.

2.1 The photoelectric effect

Whenever particles interact with matter, a large number of effects can occur that depend on the nature of the projectile particle and the target material. Massive particles are slowed down, whereas photons, as they are neutral and massless, are absorbed or diffracted. For this bachelor thesis, the most relevant effect of photons interacting with matter is the photoelectric effect.

The principle is rather simple: A photon γ moves through a target material and gets absorbed. If the energy of the photon $\hbar\omega$ (with the reduced Planck constant $\hbar$ and the angular frequency ω) is higher than the binding energy E_b of the electron e^- to the target atom A, then the electron gets ejected and leaves an ionised atom:

$$A + \gamma \rightarrow A^+ + e^- , \tag{3}$$

where the energy of the electron is $E_{e^-} = \hbar\omega - E_\mathrm{b}$.

2.2 Semiconductors and p-n junction

In case of conductivity, a distinction is made between metals (no band gap in the energy band schema, valence band and conduction band overlap), intrinsic semiconductors (small band gap in the region of few eV) and isolators (large band gap). The conductivity of semiconductors increases exponentially with higher temperatures. For $T = 0$ all electrons are located in the valence band; with higher temperatures some electrons are excited to the conduction band and leave a “hole” in the valence band. Both electrons and holes are charge carriers.

Semiconductors can be doped to enhance the conductivity what makes them extrinsic semiconductors. In the process of doping, impurity atoms are embedded in the semiconductor material to generate additional energy levels in the band schema which causes smaller energy gaps and therefore more easily excitable energy levels. A distinction is made between n-type and p-type doping, where in the former donor impurity atoms are embedded, in the latter acceptor impurity atoms. Donor impurities hold more valence electrons than the semiconductor material they are embedded in, acceptor impurities hold less.

A contact of an n-type and a p-type semiconductor layer is called a p-n junction as shown in fig. 4. Electrons from the n-type layer diffuse into the p-type layer, the holes diffuse in opposite direction. The separation of charge leads to an electric field that in turn counteracts the diffusion process. So in thermal equilibrium, a depletion layer between the two types is established.

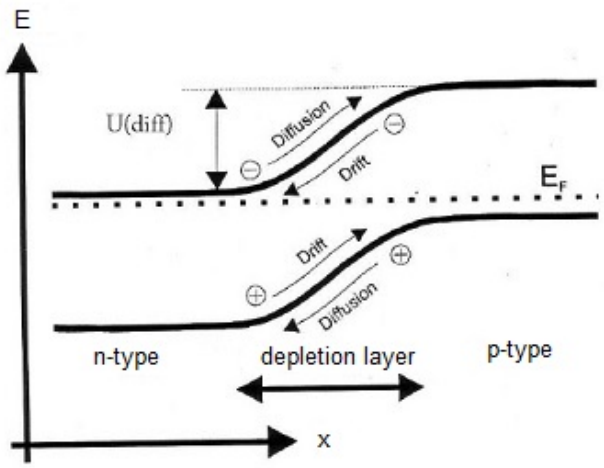

Figure 4: Schema of the p-n junction. [IMP11]

A positive potential applied to the n-type causes an extension of the depletion layer (reverse bias) whereas a positive potential applied to the p-type counteracts the diffusion potential and enables a current (forward bias). The p-n junction is the main element of semiconductor diodes.

2.2.1 LEDs

A light-emitting diode (LED), as its name implies, is a semiconductor diode that also emits light. When in forward bias mode, electrons from the p-type valence band are excited to the conduction band and move to the n-type layer where they fall back to the valence band, ergo recombine with the holes. The released energy from this process appears as light. The wavelength of the emitted light depends on the width of the band gap.

2.2.2 Photodiodes

Photodiodes are diodes in reverse bias mode that can convert light into electric pulses. If a photon impinges and its energy is higher than the width of the band gap of the semiconductor material, an electron is excited to the conduction band and leaves a hole in the valence band (inner photoelectric effect). The electron diffuses to the n-type layer, the hole to the p-type layer, which induces a photocurrent proportional to the light intensity that can be measured.

2.3 Monochromator

Most LEDs do not emit monochromatic photons but cover a certain range of wavelengths. This is rather unsuitable for our experiments, so a monochromator is used to reduce the wavelength range to a minimum, or more specifically to select a certain wavelength interval

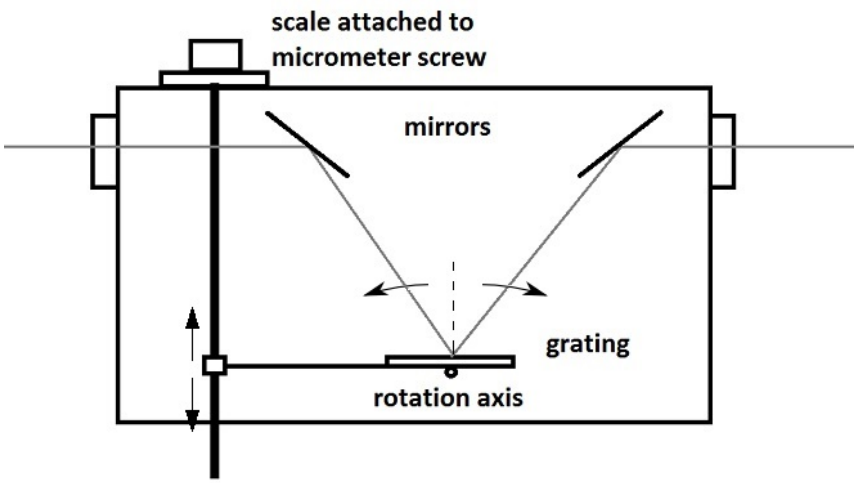

Figure 5: **Schema of the monochromator.** The path of the light beam is drawn in the figure as a grey line. [Pot13]

from the range to be used in a measurement.

The monochromator used in our setup consists of two mirrors and an optical diffraction grating as seen in fig. 5. Light entering the monochromator hits the first mirror that transmits it to the optical diffraction grating. Constructive interferences only appear for particular wavelengths and angles of incidence according to

$$n \cdot \lambda = d \cdot \sin(\varphi_n), \tag{4}$$

where n is the order of the maximum, λ is the wavelength, d is the grating constant and φ_n is the angle of incidence at which the maximum intensity occurs. The grating is rotatable via a stepper motor. By changing the angle of incidence of the light beam when rotating the grating, one particular wavelength can be selected. Afterwards, the light is transmitted to the second mirror that leads it to the monochromator exit.[4]

The LEDs in our experiment cover a wavelength range of ±5 nm around the nominal peak wavelength. The monochromator minimises this range to ±2 nm.
For more information about the monochromator used for the experiments, see the data sheet in the appendix (fig.19).

2.4 Work function

The electrons of the eGun are generated via the photoelectric effect. As described above, the photons need a minimum energy for ejecting electrons that is equivalent to the binding

[4]Described is the functionality of the monochromator used for the experiments in this bachelor thesis. There are monochromators based on other physical principles that shall not be explained here.

energy of the shell electrons. But for ejecting electrons from macroscopic surfaces like our gold layer, rather than from single atoms, there are some solid-state effects that take into account. So the binding energy differs from the energy needed for ejecting electrons from the surface. This energy is called work function and is defined with

$$w = e\phi - E_F\,, \tag{5}$$

where e is the electron charge and ϕ is the electrostatic potential in the vacuum near the surface. Therefore the product of $e\phi$ is defined as the vacuum level. The Fermi energy E_F is the highest energy a particle in a Fermi gas (in this case: electron gas) can hold if the system as a whole is in ground state. It is equivalent to the electrochemical potential μ for a temperature of $T = 0\,\mathrm{K}$. For higher temperatures, higher energy states can be occupied. The Fermi distribution gives the probability for a particle occupying a certain energy state E for a certain temperature $T > 0\,\mathrm{K}$:

$$f_{\mathrm{Fermi}}(E) = \frac{1}{\exp\left(\frac{E-\mu}{k_B T}\right)+1}\,. \tag{6}$$

Even photons with energies below the work function can eject electrons from the surface which is why the Fermi gap gets smeared out for higher temperatures.

On this basis, R. H. Fowler developed a theory of the effect of temperature on the work function of metals. An essential function used to determine the work function of our gold layer, the Fowler function, is based upon this theory. For more information and a short derivation of Fowler's theory see [Win14].

The work function of our surface can not be measured directly. The eGun's electron yield has to be measured and plotted against the wavelength of the light source. Then the measurement has to be fitted with the aforementioned Fowler function that is defined with:

$$f(\mu) = \begin{cases} e^{\mu} - \frac{1}{4}e^{2\mu} + \frac{1}{9}e^{3\mu} + \ldots & ,\ \mu \leq 0 \\ \frac{\pi^2}{6} + \frac{\mu^2}{2} - \left(e^{-\mu} - \frac{1}{4}e^{-2\mu} + \frac{1}{9}e^{-3\mu} + \ldots\right) & ,\ \mu > 0 \end{cases}. \tag{7}$$

The parameter μ of the fit, the electrochemical potential, includes the work function w:

$$\mu = \frac{1}{k_B T}\left(\frac{hc}{\lambda} - w\right), \tag{8}$$

where $h = 4.135667516 \cdot 10^{-15}\,\mathrm{eVs}$ is the Planck constant, $c = 299792458\,\mathrm{ms}^{-1}$ is the vacuum speed of light, $k_B = 8.6173324(78) \cdot 10^{-5}\,\mathrm{eVK}^{-1}$ is the Boltzmann constant [COD10], T is the temperature and λ is the wavelength. [Win14]

2.4.1 Coherence of work function and wavelength

As mentioned above, the ideal wavelength for producing zero-energy electrons with the eGun can be calculated from the work function. To do so, some basic formulae are needed:

The photon energy is given by

$$E_\gamma = \hbar\omega = h\nu \tag{9}$$

and the photon wavelength by

$$\lambda = \frac{c}{\nu}. \tag{10}$$

To produce zero-energy electrons, the photons must hold an energy E_γ that is as close as possible to the work function energy w (but not below). The minimum wavelength resulting from that assumption then is

$$\lambda = \frac{c}{\nu} = \frac{c}{E_\gamma} \cdot h = \frac{c}{w} \cdot h. \tag{11}$$

The theoretical vacuum work function of gold is $w_{\text{Au,th.}} = 5.1\,\text{eV}$ [CRC62]. We expect a lower work function of our gold photocathode though, caused by hydrogen, oxygen or dust depositions and thereby effected impureness of the layer.

2.5 Measuring errors

All measured values are never exact values. There are always inaccuracies caused by technical devices, unknown conditions or the experimenter. These inaccuracies have to be considered whenever a calculation is made with values from measurements.
The error propagation formula to calculate the errors of quantities Δx consisting of several measured values (a, b, ...) that are independent from one another is defined as:

$$\Delta x(a, b, ...) = \sqrt{\left(\frac{\partial x}{\partial a}\Delta a\right)^2 + \left(\frac{\partial x}{\partial b}\Delta b\right)^2 + ...} \tag{12}$$

Equation (12) is used for all error calculations in this bachelor thesis if not mentioned otherwise.

3 The experimental setup

3.1 The test setup

The eGun test setup at the *Institut für Kernphysik* at the WWU Münster is intended for test measurements before the eGun can be disassembled and re-installed at the KATRIN main spectrometer at the KIT in Karlsruhe. Fig. 6 gives an overview of the setup components whereas fig. 7 shows the schematic functional principle.

The setup consists of an ultra high vacuum chamber with a pressure $p \approx 10^{-7}$ mbar with the eGun flange at the one end and a detector consisting of an Si PIN diode at the other. In between, the electrons leaving the eGun are guided by the magnetic field lines of the eGun magnet with a field intensity of ≈ 10 mT and the detector magnet[5] with a field intensity of ≈ 100 mT, where the latter straitens the magnetic flux tube and focuses the electron beam on the detector.

In section 3.2 you will find an explanation of how the eGun generates electrons.

3.1.1 Light sources

To get electrons from the eGun in the first place, we need coherent monochromatic light to eject electrons from the gold layer (detailed explanation in 3.2). The light sources are assembled inside the laser box (at the rightmost side of fig. 6). For a photon source one can choose between a pulsed UV laser and a revolver containing six pulsed UV LEDs. A view inside the box is given in fig. 9. In operation mode, the laser box is shut and secured with an interlock to prevent ambient light from interfering in the measurement and to ensure safe laboratory work.

In the course of this bachelor thesis some alterations were added to the laser box[6]:

- The UV LED revolver (which was constructed by A. Potthoff [Pot13]; the missing current supply was added in the course of this bachelor thesis),
- a parallel assembly for both the laser and the LED revolver which allows a simultaneous operation of both devices,
- a second beam splitter and photodiode for monitoring the light intensity of the LED revolver.

Both light sources, the laser and the UV LED revolver, as well as the photodiode and the monochromator are controlled by LabVIEW programs developed by [Pot13] and completed in the course of this bachelor thesis.

[5] The magnets are also named Hillen-coil (eGun magnet) and Baumeister-coil (detector magnet) after their constructors.

[6] Since the laser box assembly was last described in [Win14].

Figure 6: **The eGun test setup.** (1) Grounded HV-cage, (2) eGun magnet/ Hillen-coil, (3) eGun flange, (4) detector magnet/ Baumeister-coil, (5) detector, (6) rack with power supplies and DAQ computer, (7) optical fibre coming from the laser box, (8) Ph.D. student Michael Zacher. [Pos11]

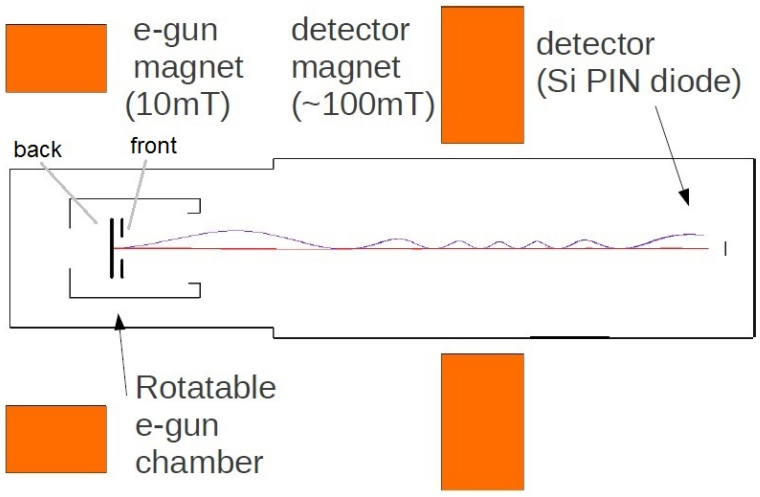

Figure 7: **The eGun test setup (schematic).** The electrons move adiabatically after passing the front plate of the eGun. The magnets focus the electron beam on the detector diode. [Zac13]

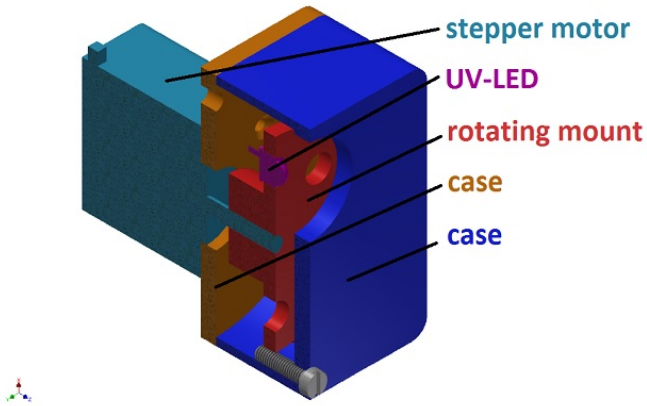

Figure 8: Schematic setup of the LED revolver. [Pot13]

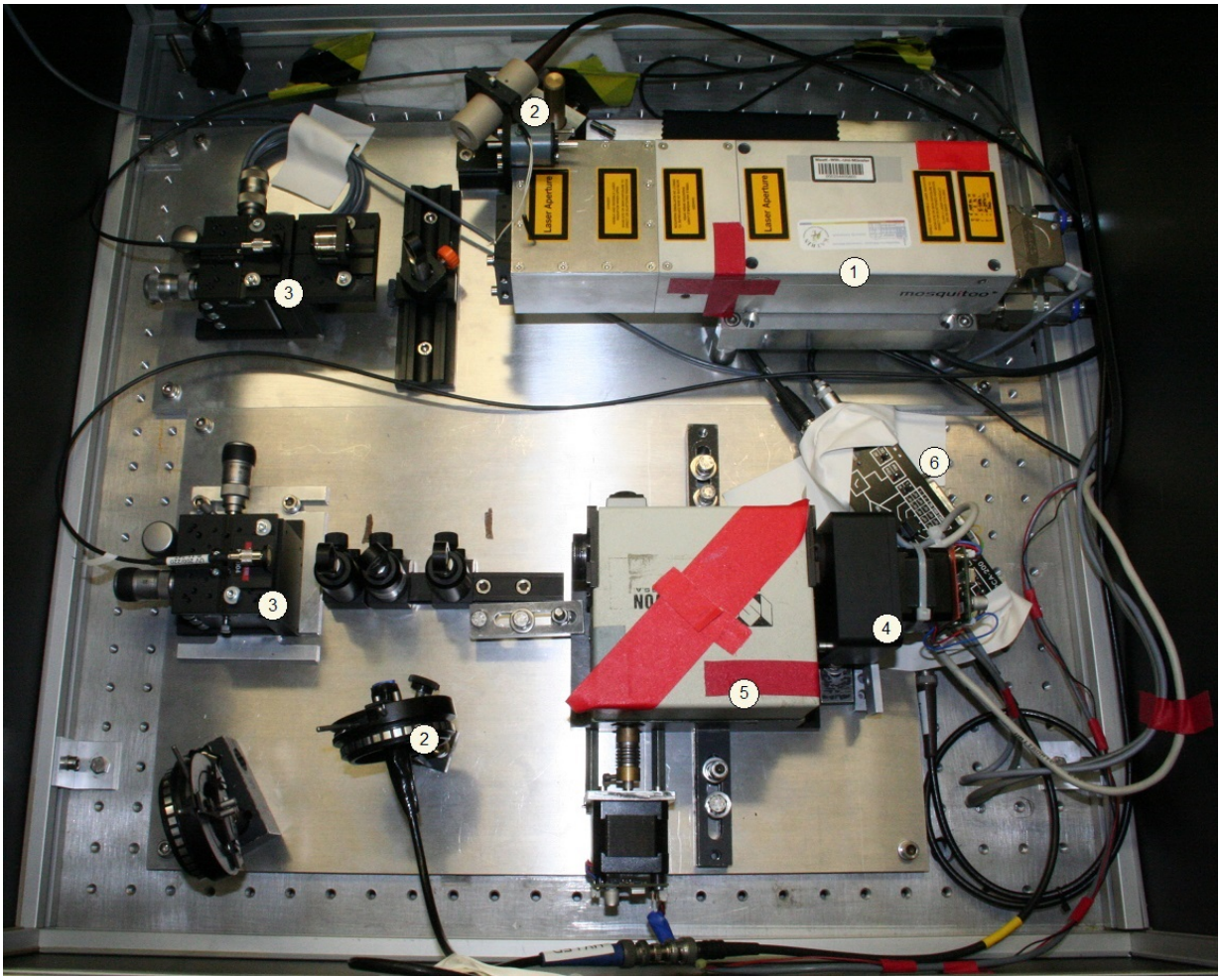

Figure 9: **The laser crate with the optical setup.** (1) Pulsed UV laser, (2) photodiode, (3) coupling to the optical fibre, (4) UV-LED revolver, (5) monochromator, (6) photodiode amplifier. [Beh14]

The Laser

The Laser is a class 4 pulsed Nd:YAG laser which emits infrared light. A wavelength of $\lambda_{\text{laser}} = 266\,\text{nm}$ in the UV range is achieved via frequency quadrupling. Since the laser is secured with an interlock switch inside the laser box (expect during setup adjustments), it can be considered class 1. The laser beam is focused by a collecting lens and coupled into the optical fibre after being split by a beam sampler that separates 0.3 % of the photons, so the light intensity can be measured by a photodiode. The intensity can be controlled by a $\lambda/2$ waveplate inside the laser or neutral density filters[7] assembled in the beam path. The laser shows strong fluctuations in light intensity though, which can be ascribed to transient effects.

The UV LED revolver

The LED revolver consists of a rotatable plate with up to eight UV LEDs attached to it. The plate is surrounded by a plastic housing with a round aperture for installing the revolver in front of the monochromator. The plate is connected to a stepper motor that can approach any desired LED to the aperture (see fig. 8).
For our experiment, 6 UV LEDs with different peak wavelengths of $\lambda_{\text{LEDs}} = 260\,\text{nm} - 310\,\text{nm}$ are installed inside the revolver[8]. The LEDs cover a range of $\pm 5\,\text{nm}$ around the nominal centre wavelength. The monochromator reduces the wavelength range of the selected LED to $\pm 2\,\text{nm}$. Behind the monochromator, the beam is focused by two collecting lenses and coupled into the optical fibre after being split by a beam sampler that separates 0.3 % of the photons, so the light intensity can be measured by a photodiode.

The LEDs are controlled by a frequency generator with the following settings:

- Pulsed mode, 100 kHz (as with the laser),
- duty cycle: $1 - 15\,\%$ (chosen for each LED so that the light intensities are roughly the same),
- voltage of 8.5 V,
- internal resistor of $50\,\Omega$.

[7] A neutral density filter (ND filter) reduces the intensity for every wavelengths of the inciding light equally [Wik14]. The ND filters used for our experiments reduce the intensity of the transmitted light to 1 % or alternatively 0.1 %.

[8] The electronics only left space for six instead of eight LEDs inside the revolver, which is sufficient for our experiments.

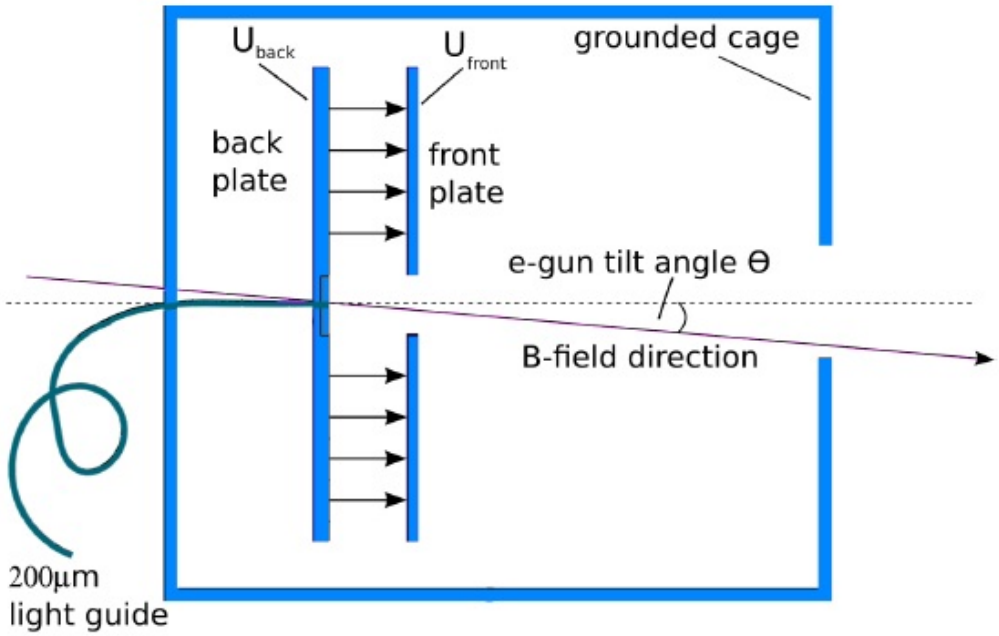

Figure 10: eGun assembly (schematic). [Zac14]

3.2 The angular selective electron gun (eGun)

The purpose of the eGun is to provide electrons for calibrating the KATRIN main spectrometer like it is described in [Win14]. The schematic technical setup is shown in fig. 10.
The eGun consists of a photocathode inside a two-plate setup similar to a plate capacitor which is set in a grounded housing. A voltage of $U_{\text{back}} = 20.1\,\text{kV}$ is applied to the back plate, a voltage of $U_{\text{front}} = 17.1\,\text{kV}$ to the front plate, which leads to an acceleration voltage of $U_{\text{acc}} = 3.0\,\text{kV}$ between the plates. UV light is guided through an optical fibre to the back plate to eject electrons from the photocathode via the photoelectric effect. The ejected electrons are accelerated non-adiabatically in the electric field inside the eGun chamber. After passing the front plate, the electrons move adiabatically along the magnetic field lines. The eGun can be tilted to measure the movement of electrons with a certain angle to the field lines (pitch angle, $\vartheta = \measuredangle(\vec{p}, \vec{B})$). For pictures of the eGun assembly see fig. 11.

The subject of this bachelor thesis is to characterise the photocathode of the eGun. The associated experiment and data analysis is given in section 5.

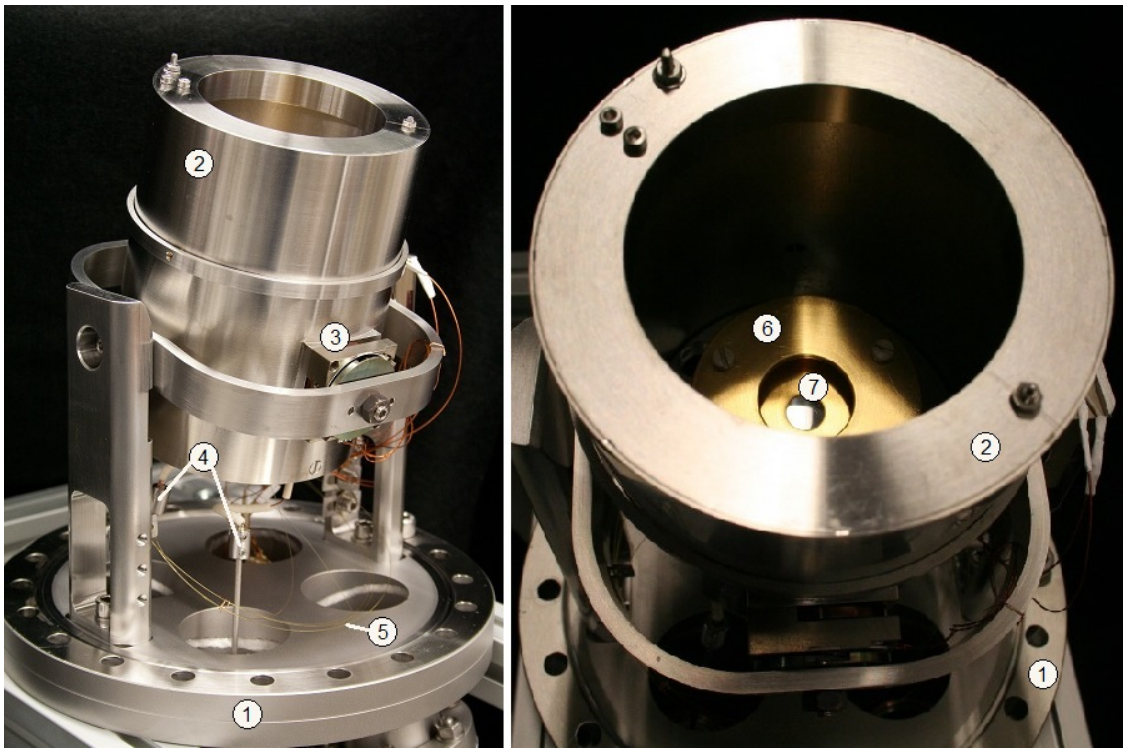

Figure 11: **EGun assembly and view inside the eGun enclosure.** (1) Vacuum flange, (2) enclosure, (3) attocube motor for position readout, (4) HV feedthrough, (5) optical fibre, (6) front plate, (7) back plate with gold layer. [Zac13]

3.2.1 The energy spectrum of the eGun electrons

Ideally, the electrons from the eGun are monoenergetic which results in a single delta peak in the energy spectrum at the detector. But ideal preconditions can not be assumed. There are some uncertainties that can not be eliminated, like

- the uncertainty of the emitted wavelengths of the light sources,
- the impurity of the gold layer which leads to electrons getting dissolved from the surface by photons with different energies,
- light postponements of the magnets or other devices that lead to misalignments of the electric and magnetic field lines,
- general inaccuracies of technical devices, especially the detector.

So the energy spectrum describes not a delta peak but a Gaussian function. The peak position depends on the acceleration voltage. Besides, there are often several peaks visible instead of just one single peak. The other peaks do not result from electrons with higher energies but from two, three or more electrons that hit the detector simultaneously, so the energy

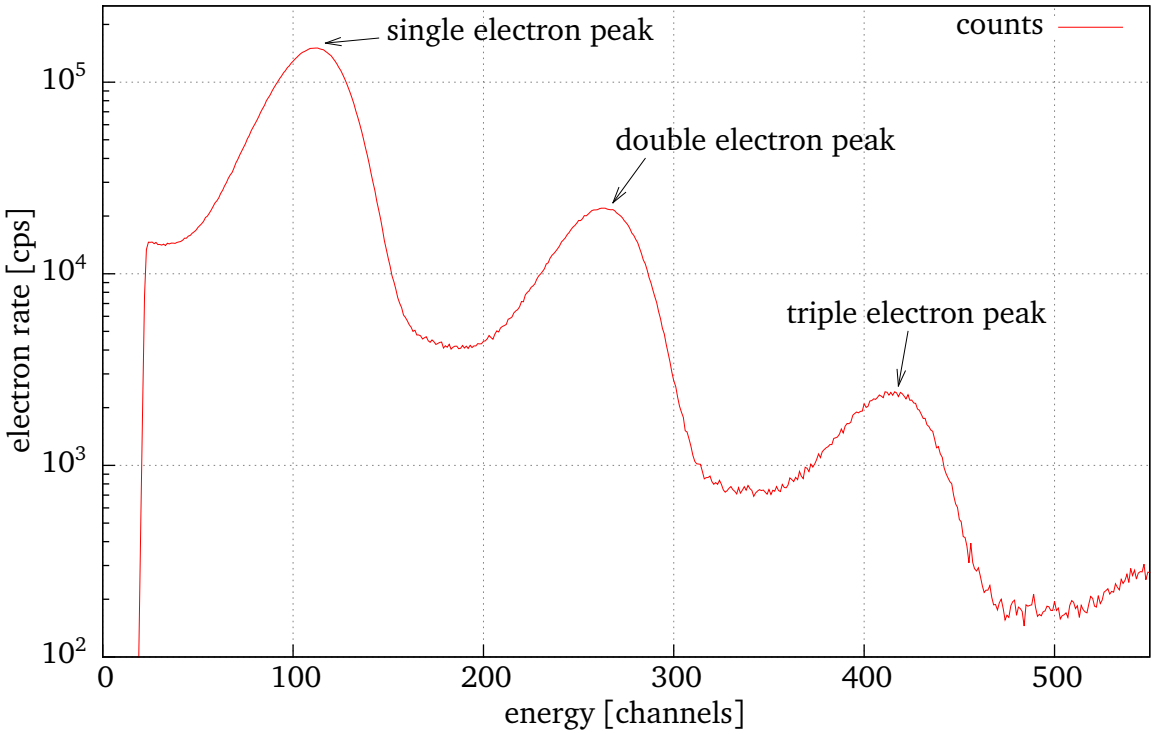

Figure 12: eGun energy spectrum.

deposition in the detector adds up. This means a particular evaluation has to be taken into account for each peak: Counts in the second peak are counted twice, in the third peak thrice and so on[9]. The peaks are considered the regions of interest (ROIs), all the other parts of the spectrum are considered noise. A sample energy spectrum can be seen in fig. 12.

For the long-term measurements in section 5.1, data was taken for several hours every day. In order to see the daily development of the electron rate, energy spectra were taken in about altogether 60 five-minute measurements per day. The electron yield per five minutes is the sum over all counts in the ROIs with the particular evaluation. The background amounts to a very low count rate of ≈ 0.5 cps, which is why a background correction is unnecessary.

[9]An evaluation is not necessary for the work function measurements, since we get only one single peak in each spectrum because of the low total count rates.

4 Calibration of the setup components

4.1 Monochromator calibration

4.1.1 Calibration by means of the laser

The monochromator has to be calibrated so that the positions of the stepper motor can be converted into wavelengths. The laser suits best for the calibration because of its defined wavelength of $\lambda_{\text{laser}} = (266 \pm 1)\,\text{nm}$.
The stepper motor is set to move the monochromator transmission window by ±10 nm around the laser wavelength. The light intensity at the monochromator exit is measured by the photodiode and saved to a logfile. The position of the stepper motor with the maximum light intensity fits to the wavelength of our laser. The measurement data can be found in fig. 13.
A Gaussian function[10] according to

$$g(x) = a \cdot \exp\left\{-\ln 2\left(\frac{x-p}{\text{FWHM}}\right)^2\right\} + c \tag{13}$$

is fitted to the data points. The relevant fit values and parameters are printed in the graph. If we put

- the wavelength of the laser $\lambda_{\text{laser}} = (266 \pm 1)\,\text{nm}$,
- the peak position of the Gaussian fit $p = (39989.9 \pm 3.1)\,\text{steps}$, which corresponds to the position of maximum light intensity,
- and the slope $s = (128.542 \pm 0.052)\,\frac{\text{steps}}{\text{nm}}$, which has been measured before and is assumed to be fixed [Pot13]

into the monochromator linear-equation

$$p \;=\; s \cdot \lambda + o\,, \tag{14}$$

the monochromator offset can be defined to

$$o_{\text{Laser}} = (5798 \pm 129)\,\text{steps}\,. \tag{15}$$

Unfortunately, this does not seem to be the correct monochromator offset. The calibration was done after the actual measurements; the measurements were supposed to be adjusted with the monochromator offset retrospectively. These adjustments lead to wrong results: The measured peak wavelengths of the UV LEDs clearly aberrates the peak wavelengths given on the LED's data sheets. So the monochromator offset is assumed to be shifting over time, for example during setup adjustments (the LED revolver had to be disassembled from the

[10] We assume that the light coming from both the laser and the monochromator has a Gaussian wavelength distribution. The convolution of both gaussion functions is a wider gaussion function with the same peak position.

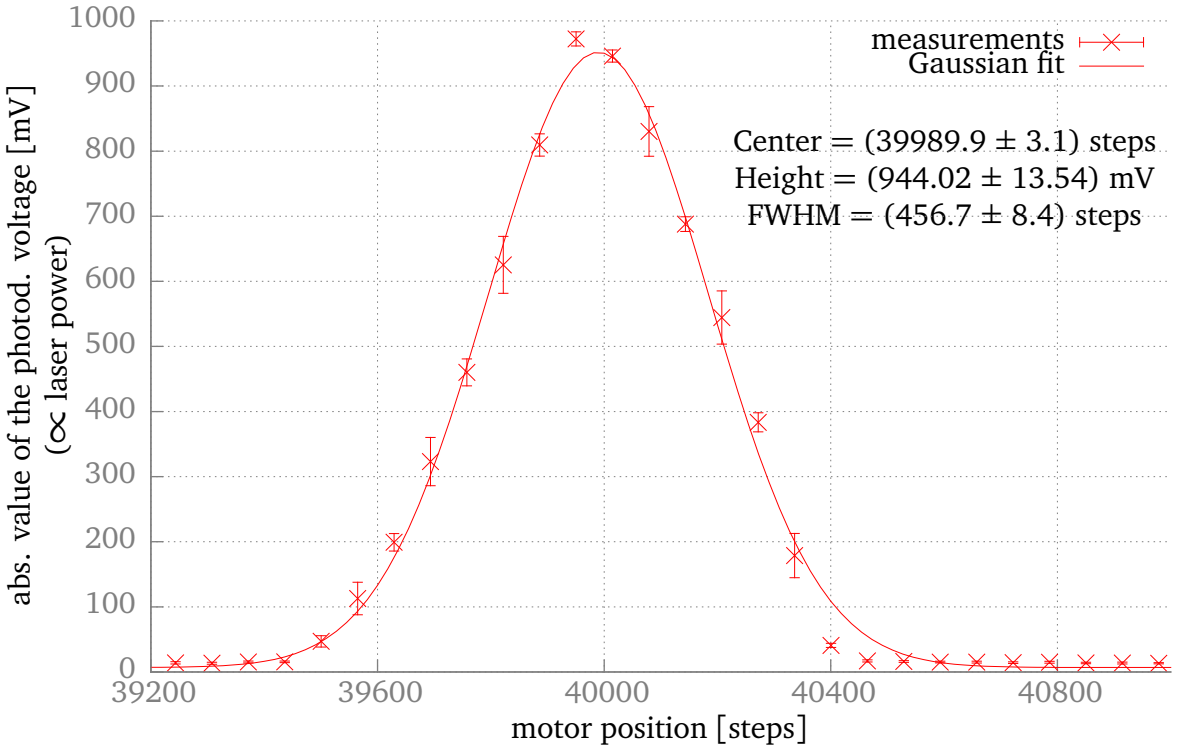

Figure 13: Measurement curve for the monochromator calibration.

monochromator so that the laser could take its place; during this process the monochromator had to be screwed off and moved several times).
The monochromator is again calibrated by the UV LEDs, which is described in the next section.

4.1.2 Calibration by means of the UV LEDs

As mentioned above, the LEDs do not have a defined wavelength but cover a range of ±10 nm around the nominal peak wavelengths that are given in each LED's data sheet[11] (see appendix fig. 20 and 21). To find the correct monochromator offset, the motor position with the maximum light intensity has to be determined for each LED. The procedure is similar to the one in the previous section:
The stepper motor is set to move the monochromator transmission window by ±10 nmaround the nominal centre wavelength of each LED. The light intensity is again measured by the photodiode and saved to a logfile. The motor positions with the maximum light intensity $p_{\max}$ for all six UV LEDs can be determined from the plots in fig. 22 and 23 in the appendix and are given in table 1. These positions are assumed to correlate to the nominal peak wavelengths λ_{nom}, so the monochromator offset for each LED can be calculated by means of

[11] To avoid confusion: The nominal peak wavelength of each LED differs from the number in the LED's name; e.g.: The UVTOP260 has a nominal peak wavelength of 264 nm.

equation (14) which can be formed to

$$o_{\mathrm{LED}} = p_{\mathrm{max}} - s \cdot \lambda_{\mathrm{nom}} \,. \tag{16}$$

The mean offset results to

$$\bar{o}_{\mathrm{LED}} = (5292 \pm 106)\,\mathrm{steps}\,. \tag{17}$$

This monochromator offset is assumed to be the actuel offset for all LED measurements, because the monochromator was not moved or disassembled any more during the whole measurement period.

LED #	name	$\lambda_{\mathrm{nom.}}$ [nm]	p_{max} [steps]	o [steps]
LED 2	UVTOP260	265 ± 2	39396 ± 4	5332 ± 258
LED 3	UVTOP270	275 ± 2	40452 ± 3	5103 ± 258
LED 4	UVTOP280	285 ± 2	41733 ± 2	5099 ± 258
LED 5	UVTOP290	295 ± 2	43529 ± 2	5609 ± 258
LED 6	UVTOP300	305 ± 2	44522 ± 2	5317 ± 258
LED 7	UVTOP310	315 ± 2	45785 ± 2	5294 ± 258
				$\bar{o}_{\mathrm{LED}} = 5292 \pm 106$

Table 1: **Nominal peak wavelength λ_{nom}, motor position with maximum light intensity p_{max} and associated monochromator offset for each UV LED.** The error of λ_{nom} is given in the data sheets.

5 Characterisation of the eGun-photocathode

5.1 Long-term measurements

In this first experiment, the durability of the gold photocathode is to be determined. For this purpose, the eGun's electron rate is measured and recorded over a period of several weeks to gain information about the long-term behaviour and stability of the gold layer.
A behaviour similar to the former silver photocathode is expected:

"*Due to the negative potential on the backplate and the silver substrate, the surface of the silver is subject to bombardment by positive ions produced by ionization of restgas molecules in the vacuum chamber. This leads to a change in the thickness of the silver over time. Additionally the surface composition of the adsorbates on the silver surface changes over time after installing the electron gun in the vacuum chamber. At the beginning of a measurement phase the surface composition will still be dominated by adsorbates adsorbed under atmospheric conditions, whereas after a some time in the vacuum chamber the surface composition will change. [...] It is not clear which of the effects described before is dominant for the rate progression that was observed*." [Win14]

The electron rate progression from the silver plate over 28 days is shown in fig. 14.

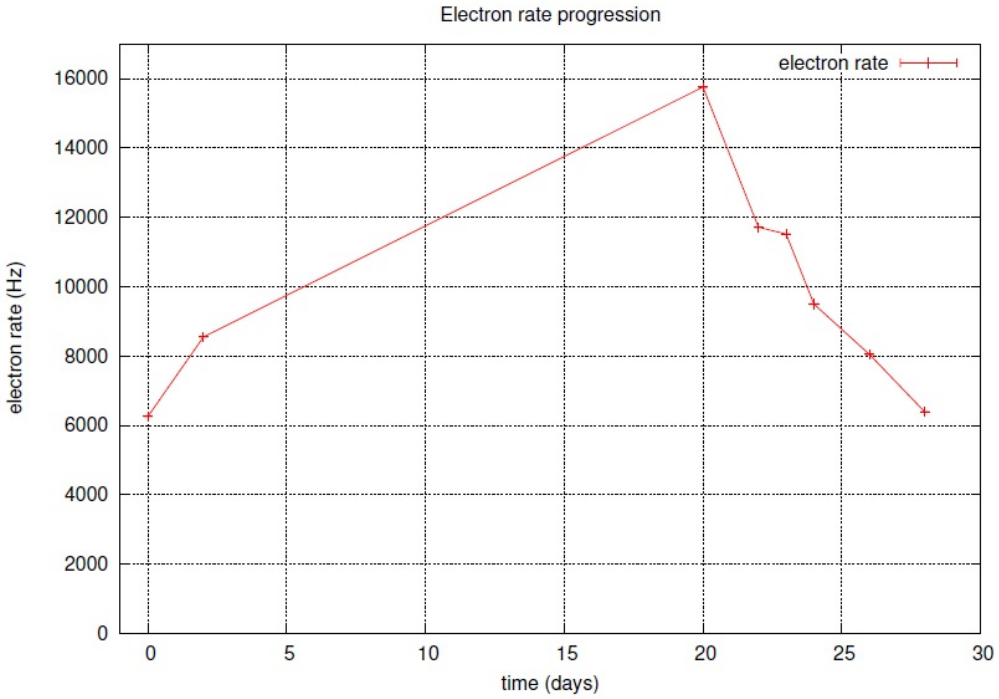

Figure 14: **Photoelectron rate progression of the eGun with installed silver photocathode over 28 days.** The data points are connected for better visibility. [Win14]

The following settings are used for all measurements with the gold photocathode (for eGun test setup commissioning see section 3):

- High voltage: $U_{\text{back}} = 19.8\,\text{kV}$, $U_{\text{front}} = 16.8\,\text{kV} \quad \Rightarrow \quad U_{\text{acc}} = 3.0\,\text{kV}$
- eGun magnet: $I_{\text{Hillen}} = 21\,\text{A}$
- Detector magnet: $I_{\text{Baumeister}} = 100\,\text{A}$

The laser suits best for the measurement because of its higher light intensity and therefore higher electron rate which leads to less statistical measurement errors.

Measurements were taken for altogether 21 days within two months, as shown in fig. 15 and 16. A clear increase in the photoelectron rate progression can be seen during the first measurement phase in February. After 12 days the measurement had to be suspended for technical reasons (installing of the beam splitter and the photodiode). Unfortunately, the count rate of the further measurements was not comparable to the first data any more after re-adjusting the optical setup. But since the eGun was not exposed to air during the setup alterations, the progression of the rate remained unaffected. The electron rate was much lower afterwards, mainly because the light intensity coupled into the optical fibre changed; and showed a constant progression, see fig. 15, upper graph. In the lower graph, the data was averaged over the several days and the measurements taken after altering the setup were adjusted so they match to the previous data for better visibility. These adjustments are based upon the assumption that only the count rate changed but the progression of the rate remained unaffected. This assumption can not be completely verified though.

Taking a closer look at fig. 15, upper graph, each day-measurement shows a distinct trend over the day. This can be explained with transient effects of the laser. The same trends can also be seen in fig. 16. At this point of time, the read out software for the photodiode (which was installed after 12 days) was not ready for operation yet, so the measurements could not be normalized by the light intensity.

After the second measurement phase that lasted till February 27th, the setup had to be re-assembled once again for problems caused by the detector magnet. Another measurement series was run for a few days in march. The electron rate was relatively poor though in comparison to the February measurements, see fig. 16 (please note that the scale of the count rate axis is now in [cps] instead of [kcps]). The reasons behind the poor rate are deficient coupling of the optical fibre and probably some displacements of the magnet and the eGun itself that could not be corrected at that time. Besides, the setup had to be vented to normal pressure and further impurities were probably added to the gold layer, which could also have influenced the electron rate. So unfortunately, the new measurements are again not directly comparable to the old ones. A similar slope is observable though, see the parameter m in both graphs. If normalized by the maximum electron rate, the slopes result to

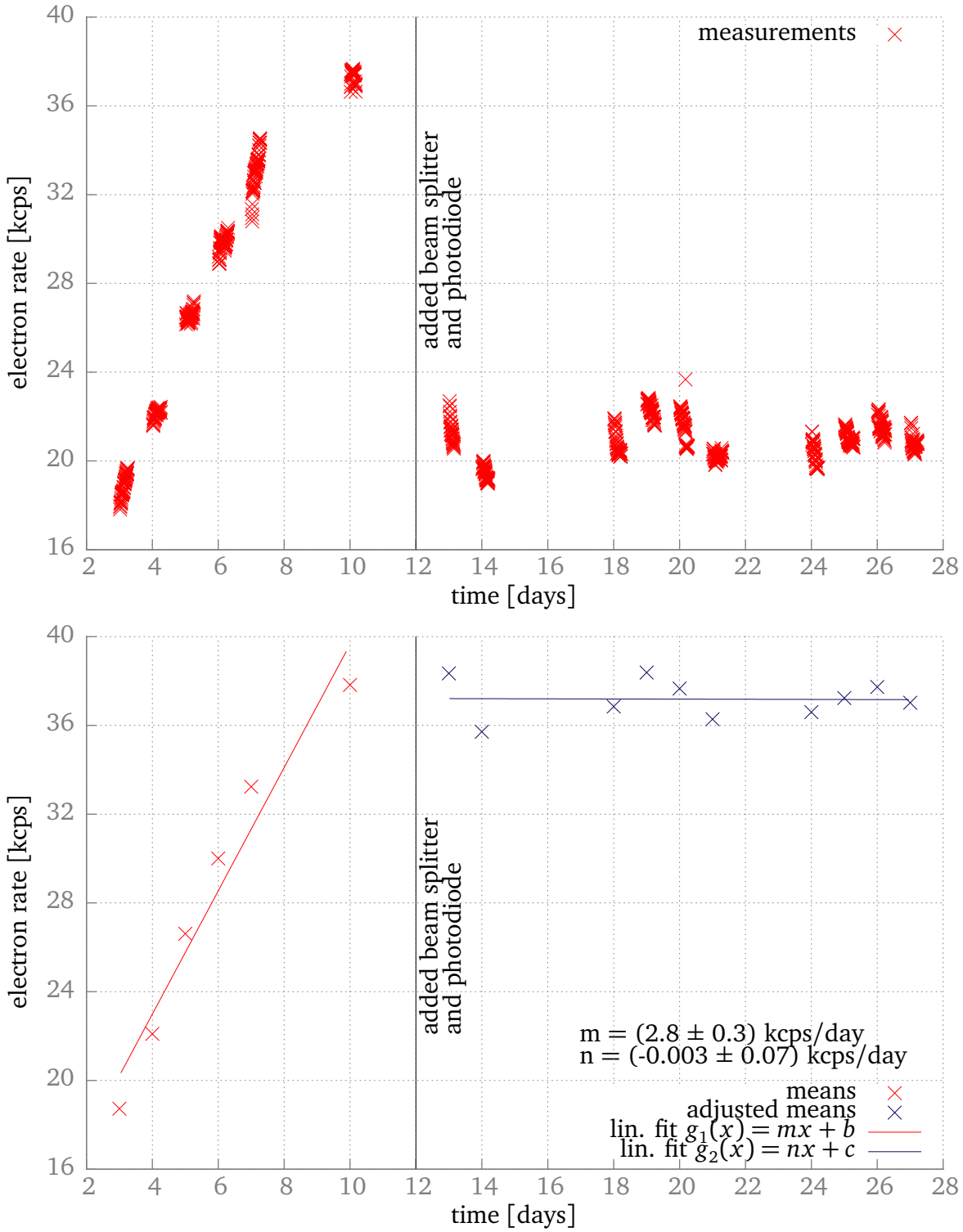

Figure 15: **Photoelectron rate progression of the eGun in February.** The line at day 12 marks the installation of the beam splitter and the photodiode. Upper graph: Plot with all measurements. Lower graph: Average daily photoelectron rates with adjusted measurements.

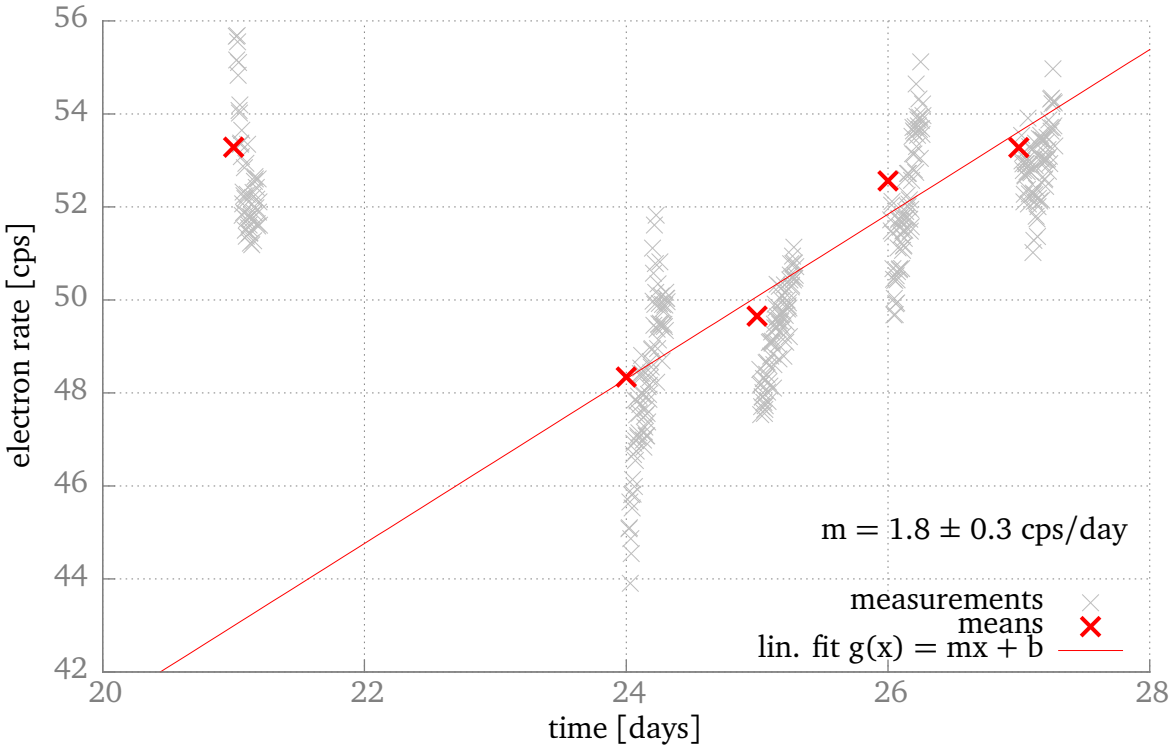

Figure 16: **Photoelectron rate progression of the eGun in March.** The grey data points represent the measurements, the red data points represent the average daily electron rate. The first measurement is assessed as an outlier and is not taken into account for the fit.

$$m_{\text{Feb}} = 0.07\,\text{days}^{-1}, \tag{18}$$

$$m_{\text{Mar}} = 0.03\,\text{days}^{-1}. \tag{19}$$

Before first measurements were taken in February, the gold layer was stored under normal pressure, too. So the similar slopes could suggest a similar behaviour of the gold layer after being exposed to air.

The expected instabilities in the electron rate that has been observed before for the silver layer did not eventuate. Especially the constant progression from February 13th to 27th indicates a good long term stabilty of the gold photocathode.

5.2 Work function measurements

To characterise the eGun photocathode, the specific work function of the gold layer has to be determined. In theory, gold has a vacuum work function of $w_{\text{Au,th.}} = 5.1\,\text{eV}$ [CRC62] under laboratory conditions. The work function of our gold layer is expected to be lower, caused by hydrogen-, oxygen- or dust depositions and thereby effected impureness of the layer. According to the Fowler theorem, the work function can be determined by measuring the photoelectron yield as a function of the wavelength. For all measurements the following settings (that are optimized to the maximum count rate) are used:

- High voltage: $U_{\text{back}} = 20.1\,\text{kV}$, $U_{\text{front}} = 17.1\,\text{kV} \quad \Rightarrow \quad U_{\text{acc}} = 3.0\,\text{kV}$
- eGun magnet: $I_{\text{Hillen}} = 21\,\text{A}$
- Detector magnet: $I_{\text{Baumeister}} = 99\,\text{A}$

The livetime of each measurement is chosen so that the electron rate has about $n = 1000$ counts to minimize the statistical error $\sqrt{n}$ within reasonalbe measurement time[12]. That leads to livetimes of 8000 s or more for larger wavelengths around 300 nm, because the number of electrons that get ejected from the cathode decreases drastically for lower photon energies.

In fig. 17 you can see the electron rate and the corresponding photon intensity as a function of the LED wavelength. In fig. 18, the electron rate is normalized by the photon intensity and the quantum efficiency of the photodiode. In the upper graph, the resulting electron yield is plotted against the wavelength. To the measurements a Fowler function according to (7) is fitted. The relevant fit values and parameters are printed in the graph.

On first attempt, statistical error was underestimated which lead to small error bars and a large χ^2. So the error bars were afterwards adjusted with the square root of the original χ^2. This makes $\chi^2 = 1$ and gives the error bars a reasonable size. These adjustments are allowed if the statistical error of the measurements is the decisive factor (compared to systematical errors). This can be verified by means of the fit residuals printed in the middle graph. These residuals are normally distributed as one can see in the lower graph, where a Gaussian function is fitted to the histogram of the fit residuals. The normal distribution indicates the statistical error. The measurements in fig. 18 are printed with adjusted error bars.

As you can see in fig. 18, the work function of our gold photocathode results from the fit to

$$w_{\text{Au}} = (4.258 \pm 0.062)\,\text{eV}\,, \tag{20}$$

which is about 0.9 eV lower than the theoretical $w_{\text{Au,th.}} = 5.1\,\text{eV}$ for pure gold. Therefore the minimum wavelength of the photons to eject electrons from the gold photocathode results with (11) to

$$\lambda_{\text{Au}} = (291.18 \pm 4.24)\,\text{nm}\,. \tag{21}$$

[12]The relative error of $1/\sqrt{n}$ shows only a very slow decrease for large n.

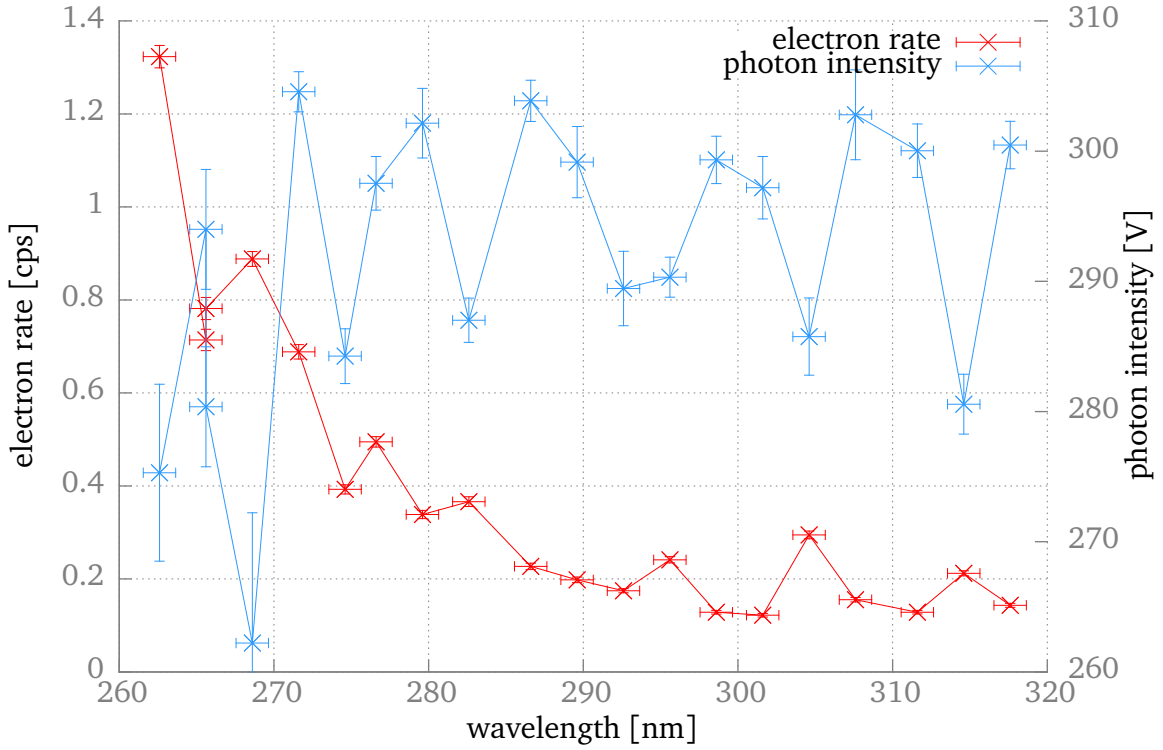

Figure 17: **Electron count rate (red) and corresponding photon intensity (blue)**. The data points are connected for better visibility.

For a gold layer with $w_{\text{Au,th.}}$, the minimum wavelength would be

$$\lambda_{\text{Au,th.}} = 243\,\text{nm} \tag{22}$$

which is about 48 nm below λ_{Au}.

For the former installed silver photocathode, a work function of $w_{\text{Ag}} = 3.9\,\text{eV} - 4.0\,\text{eV}$ could be determined [Win14]. This differs from the theoretical value $w_{\text{Ag,th.}} = 4.26\,\text{eV}$ [CRC62] by $0.26\,\text{eV} - 0.36\,\text{eV}$ which is a much smaller difference than for the gold measurements. This would indicate a much larger influence of the adsorbates to the gold layer work function than to the silver layer work function.

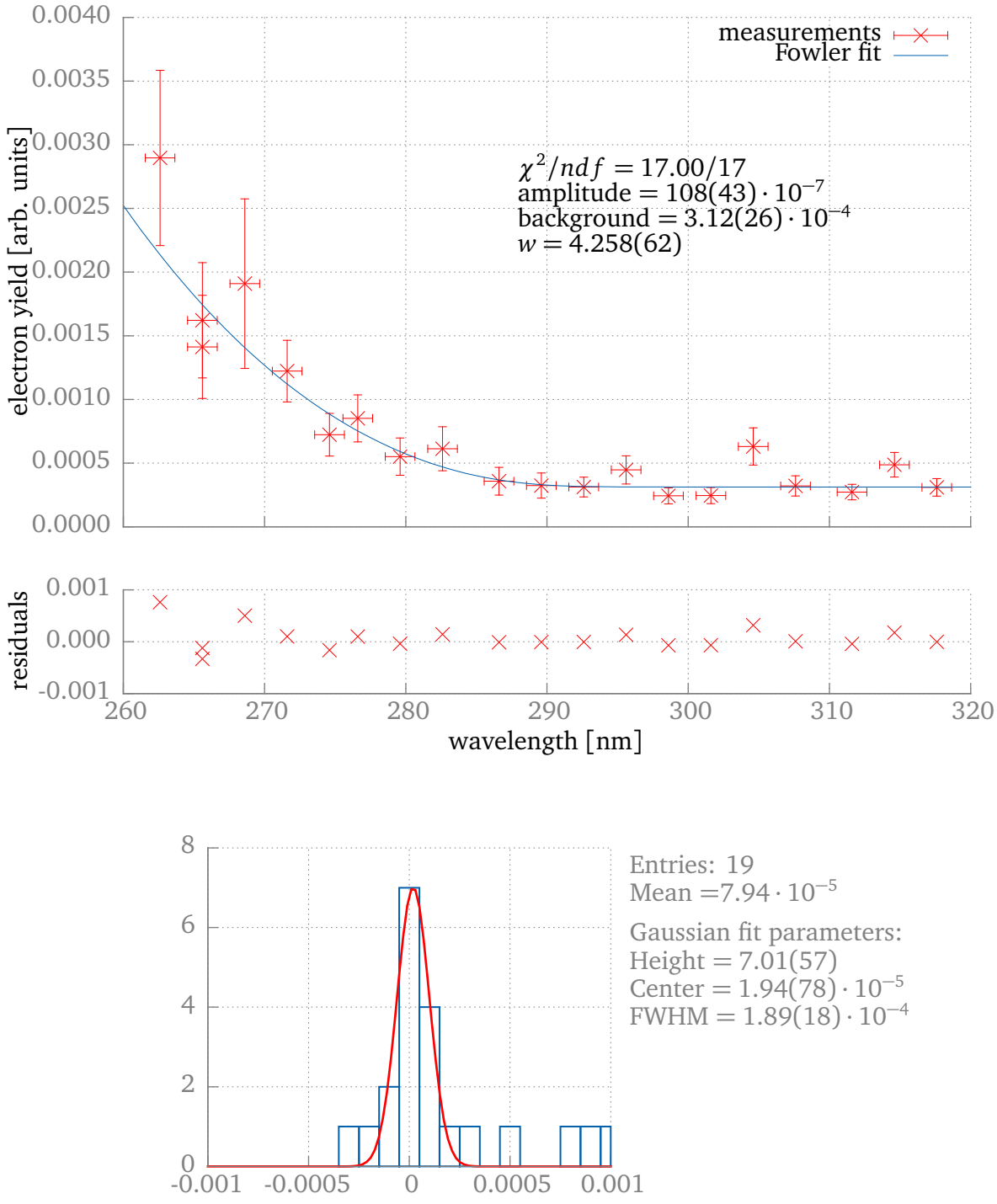

Figure 18: Upper graph: Photoelectron yield with Fowler fit to determine the work function of the gold photocathode. Middle graph: Fit residuals. Lower graph: Histogram of the fit residuals with Gaussian fit.

6 Summary and Outlook

The purpose of this bachelor thesis was to characterise the gold photocathode of the eGun, the angular selective electron source for the KATRIN experiment, which is built in order to calibrate the KATRIN main spectrometer.

The process of the characterisation contained a long-term measurement in order to test the durability and the long-term behaviour of the new gold photocathode, and a measurement to determine the work function of the surface layer.

For the long-term measurement, data was taken over a period of several weeks with the following results: The eGun was exposed to air twice during the measurement phase, once before being installed in the setup and again when the setup had to be reassembled due to some technical problems after four weeks of measurement. Whenever being stored under normal pressure, the gold photocathode showed a consistent behaviour in the form of a clear increase in the electron rate afterwards. After 12 days of increase, a constant progression was observable which suggests a good long-term stability of the gold photocathode.

To determine the work function of the gold layer, the eGun electron yield was measured as a function of the wavelength. With a Fowler function fitted to the measurements the electrochemical potential and thereby the work function could be determined to

$$w_{\mathrm{Au}} = (4.258 \pm 0.062)\,\mathrm{eV}\,,$$

which is lower than the theoretical value of $w_{\mathrm{Au,th.}} = 5.1\,\mathrm{eV}$ as we expected and as it was observed for the silver photocathode. The difference from the theoretical value by about 0.9 eV is larger than for the silver photocathode, which indicates a larger influence of the adsorbates to the gold layer work function than to the silver layer work function.
With the work function determined, the ideal wavelength of the photons to produce zero-energy electrons with the eGun could be calculated to

$$\lambda_{\mathrm{Au}} = (291.18 \pm 4.24)\,\mathrm{nm}\,.$$

Although several problems occurred during the measurements, the new gold photocathode of the eGun was successfully characterised. The results of this bachelor thesis indicate that gold suits well as a photocathode material and can be used in good conscience for the calibration measurements at the KATRIN main spectrometer. With the new fibre and some other small upgrades, the eGun will be reassembled at the main spectrometer in summer 2014.
In the course of this Bachelor thesis, the UV LED revolver was completed and is now ready for operation. The optical setup with the eGun light sources was upgraded and revised with the help of Dipl.-Ing. Hans-Werner Orthjohann and other involved technicians. For controlling the optical devices, the associated LabVIEW software, created by Alexander Potthoff [Pot13], was completed and will be used for all further calibration measurements.

In July 2014, the work function of the gold photocathode was again measured at the KATRIN monitor spectrometer in Karlsruhe, see [Rep14]. These measurements resulted in a work function of $w \approx 3.85\,\text{eV}$, which implies that the work function of our gold layer changes drastically over time. The thereby caused broader energy distribution of the electrons would lead to broader transmission functions in the main spectrometer calibration measurements, which would make it very difficult to determine the actual transmission width. Further measuremtens will show whether the gold photocathode is after all suitable for the calibration of the KATRIN main spectrometer.

7 Appendix

Specifications	H10
Focal length	100 mm
Aperture ratio	f / 3.5
Grating size	32 X 32 mm
Linear dispersion with 1200 g/mm grating	8 nm / mm
Bandpass with standard slits (0.5, 1.0, 2.0 mm) and 1200 g/mm grating	4, 8, 16 nm
Resolution with 0.1 mm slits, 1200 g/mm grating	1.0 nm
Stray light rejection, 8 bandpasses from laser, and integrated light at 230 nm, with 270 nm cutoff filter and 150 W xenon lamp	10^{-5} @ 8 band-passes from laser ≤ .5% integrated at 230 nm.
Wavelength accuracy (linearity over 500 nm range, with 1200 g/mm)	± 1.0 nm
Reproducibility with 1200 g/mm grating and backlash corrected with motor drive	± 0.25 nm
Weight	2 Kg (4.5 lb.)

Figure 19: Data sheet of the Horiba H10 monochromator. An 0,5 mm standard slit is used so the transmission window covers ±2 nm. [HoH10]

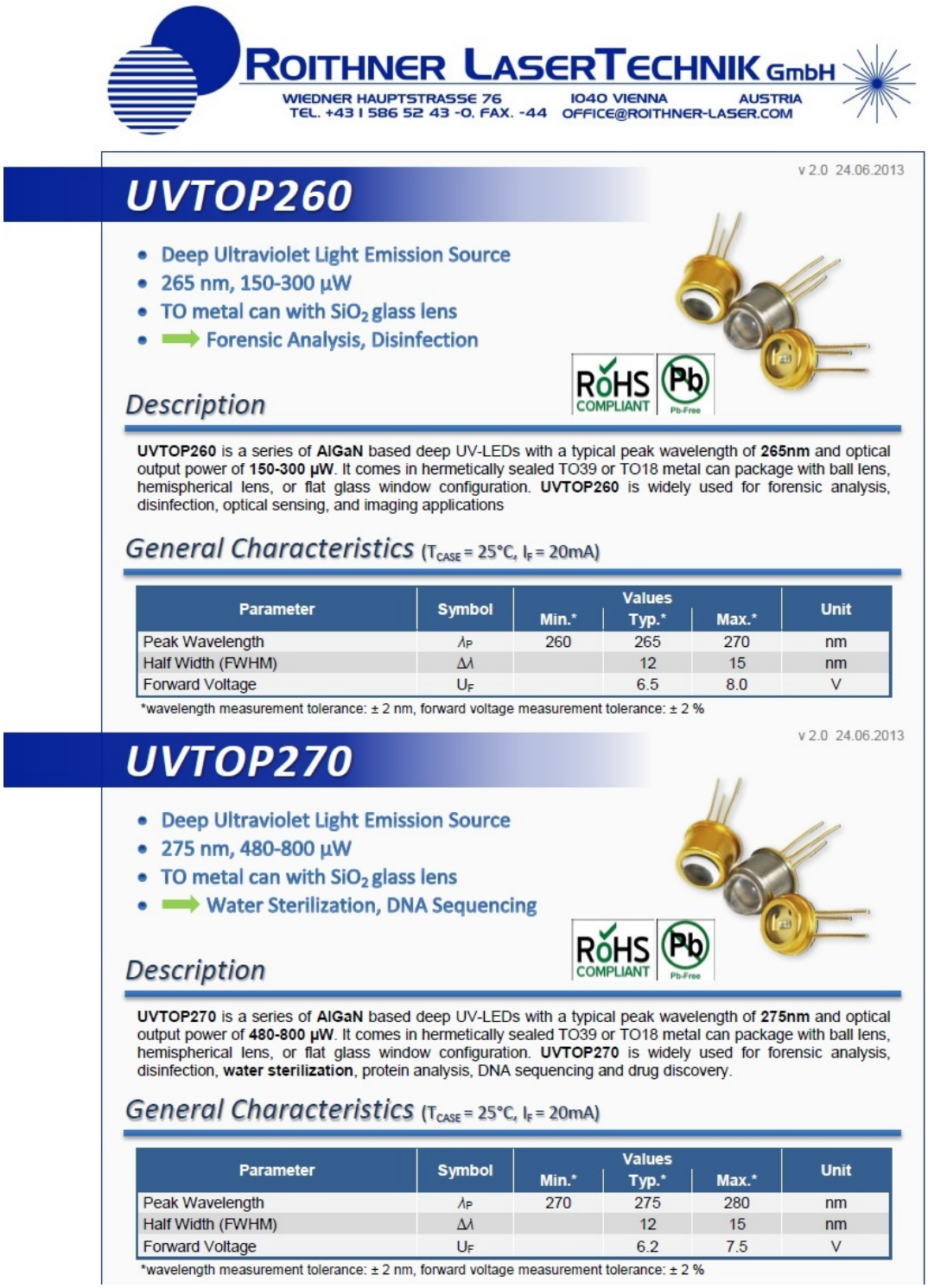

ROITHNER LASERTECHNIK GmbH
WIEDNER HAUPTSTRASSE 76 1040 VIENNA AUSTRIA
TEL. +43 1 586 52 43 -0, FAX. -44 OFFICE@ROITHNER-LASER.COM

v 2.0 24.06.2013

UVTOP260

- Deep Ultraviolet Light Emission Source
- 265 nm, 150-300 µW
- TO metal can with SiO_2 glass lens
- ➡ Forensic Analysis, Disinfection

RoHS COMPLIANT Pb Pb-Free

Description

UVTOP260 is a series of **AlGaN** based deep UV-LEDs with a typical peak wavelength of **265nm** and optical output power of **150-300 µW**. It comes in hermetically sealed TO39 or TO18 metal can package with ball lens, hemispherical lens, or flat glass window configuration. **UVTOP260** is widely used for forensic analysis, disinfection, optical sensing, and imaging applications

General Characteristics (T_{CASE} = 25°C, I_F = 20mA)

Parameter	Symbol	Values Min.*	Typ.*	Max.*	Unit
Peak Wavelength	λ_P	260	265	270	nm
Half Width (FWHM)	$\Delta\lambda$		12	15	nm
Forward Voltage	U_F		6.5	8.0	V

*wavelength measurement tolerance: ± 2 nm, forward voltage measurement tolerance: ± 2 %

v 2.0 24.06.2013

UVTOP270

- Deep Ultraviolet Light Emission Source
- 275 nm, 480-800 µW
- TO metal can with SiO_2 glass lens
- ➡ Water Sterilization, DNA Sequencing

RoHS COMPLIANT Pb Pb-Free

Description

UVTOP270 is a series of **AlGaN** based deep UV-LEDs with a typical peak wavelength of **275nm** and optical output power of **480-800 µW**. It comes in hermetically sealed TO39 or TO18 metal can package with ball lens, hemispherical lens, or flat glass window configuration. **UVTOP270** is widely used for forensic analysis, disinfection, **water sterilization**, protein analysis, DNA sequencing and drug discovery.

General Characteristics (T_{CASE} = 25°C, I_F = 20mA)

Parameter	Symbol	Values Min.*	Typ.*	Max.*	Unit
Peak Wavelength	λ_P	270	275	280	nm
Half Width (FWHM)	$\Delta\lambda$		12	15	nm
Forward Voltage	U_F		6.2	7.5	V

*wavelength measurement tolerance: ± 2 nm, forward voltage measurement tolerance: ± 2 %

Figure 20: Data sheet of the UVTOP260 and UVTOP270 LEDs (extracts). [UVT14]

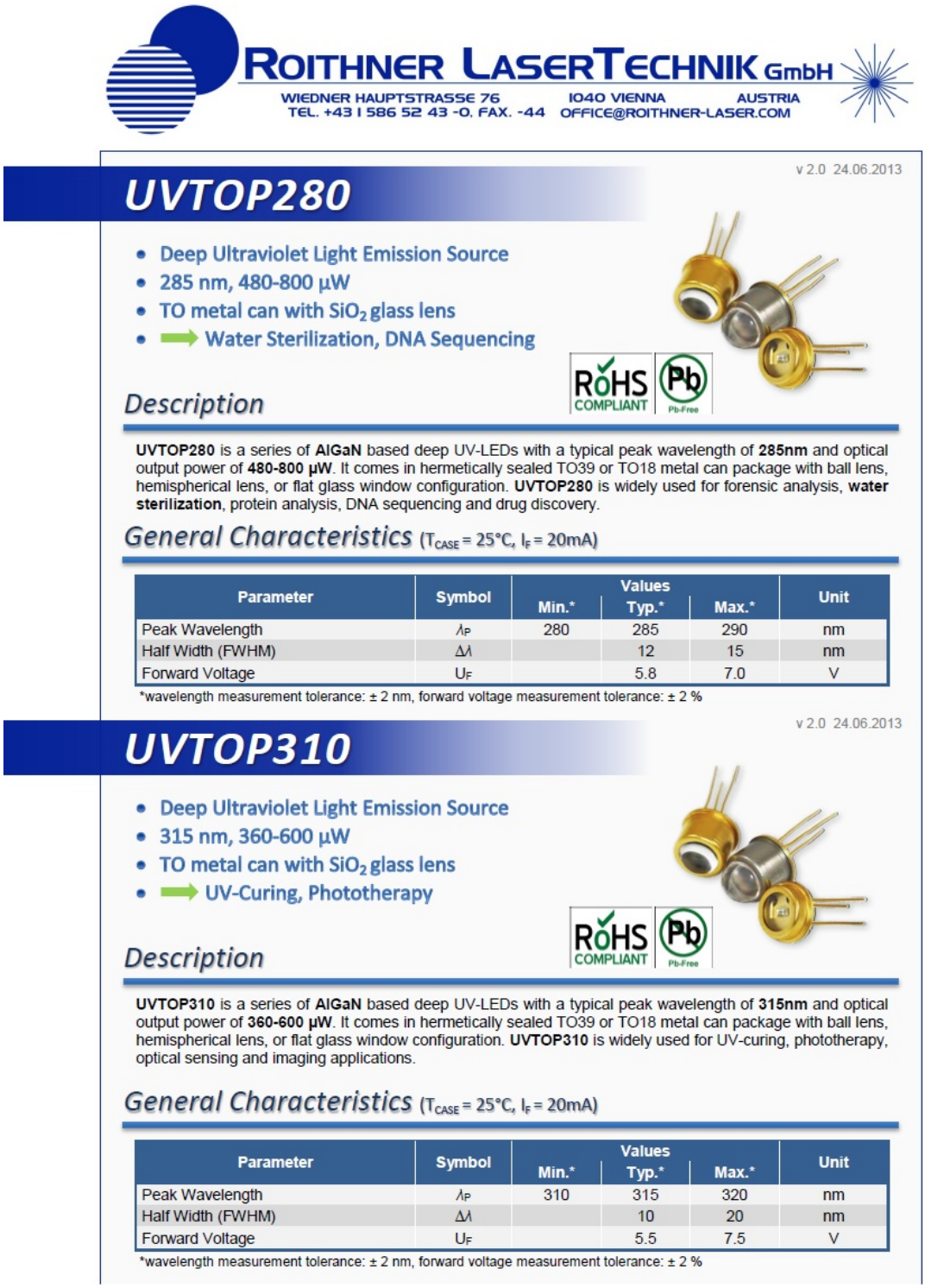

ROITHNER LASERTECHNIK GmbH
WIEDNER HAUPTSTRASSE 76 1040 VIENNA AUSTRIA
TEL. +43 1 586 52 43 -0, FAX. -44 OFFICE@ROITHNER-LASER.COM

v 2.0 24.06.2013

UVTOP280

- Deep Ultraviolet Light Emission Source
- 285 nm, 480-800 µW
- TO metal can with SiO_2 glass lens
- ➡ Water Sterilization, DNA Sequencing

RoHS COMPLIANT Pb Pb-Free

Description

UVTOP280 is a series of **AlGaN** based deep UV-LEDs with a typical peak wavelength of **285nm** and optical output power of **480-800 µW**. It comes in hermetically sealed TO39 or TO18 metal can package with ball lens, hemispherical lens, or flat glass window configuration. **UVTOP280** is widely used for forensic analysis, **water sterilization**, protein analysis, DNA sequencing and drug discovery.

General Characteristics (T_{CASE} = 25°C, I_F = 20mA)

Parameter	Symbol	Values Min.*	Typ.*	Max.*	Unit
Peak Wavelength	λ_P	280	285	290	nm
Half Width (FWHM)	$\Delta\lambda$		12	15	nm
Forward Voltage	U_F		5.8	7.0	V

*wavelength measurement tolerance: ± 2 nm, forward voltage measurement tolerance: ± 2 %

v 2.0 24.06.2013

UVTOP310

- Deep Ultraviolet Light Emission Source
- 315 nm, 360-600 µW
- TO metal can with SiO_2 glass lens
- ➡ UV-Curing, Phototherapy

RoHS COMPLIANT Pb Pb-Free

Description

UVTOP310 is a series of **AlGaN** based deep UV-LEDs with a typical peak wavelength of **315nm** and optical output power of **360-600 µW**. It comes in hermetically sealed TO39 or TO18 metal can package with ball lens, hemispherical lens, or flat glass window configuration. **UVTOP310** is widely used for UV-curing, phototherapy, optical sensing and imaging applications.

General Characteristics (T_{CASE} = 25°C, I_F = 20mA)

Parameter	Symbol	Values Min.*	Typ.*	Max.*	Unit
Peak Wavelength	λ_P	310	315	320	nm
Half Width (FWHM)	$\Delta\lambda$		10	20	nm
Forward Voltage	U_F		5.5	7.5	V

*wavelength measurement tolerance: ± 2 nm, forward voltage measurement tolerance: ± 2 %

Figure 21: Data sheet of the UVTOP280 and UVTOP310 LEDs (extracts). The UVTOP290 and UVTOP300 data sheets are not available on the Roithner Lasertechnik GmbH webpage. It is referred to the LED data sheet with the next adjacent wavelength instead. [UVT14]

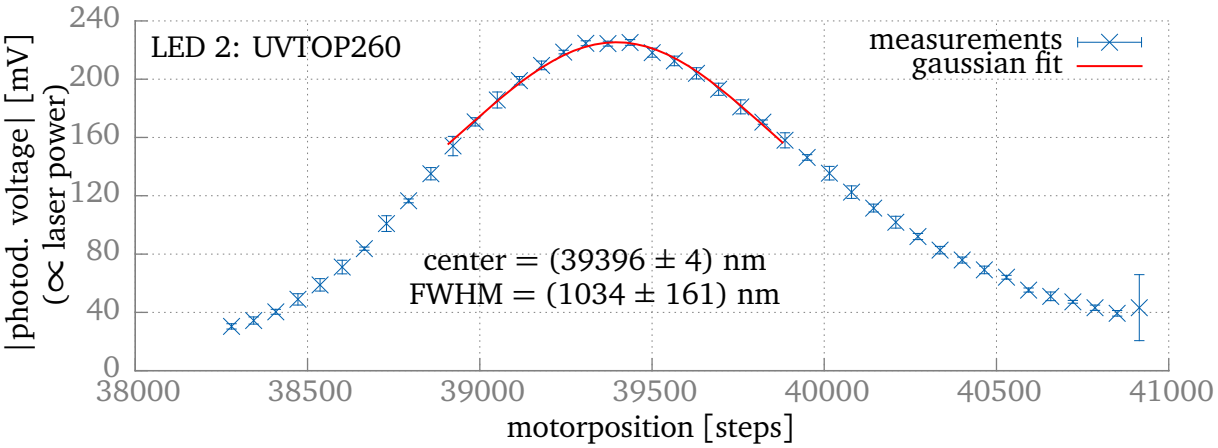

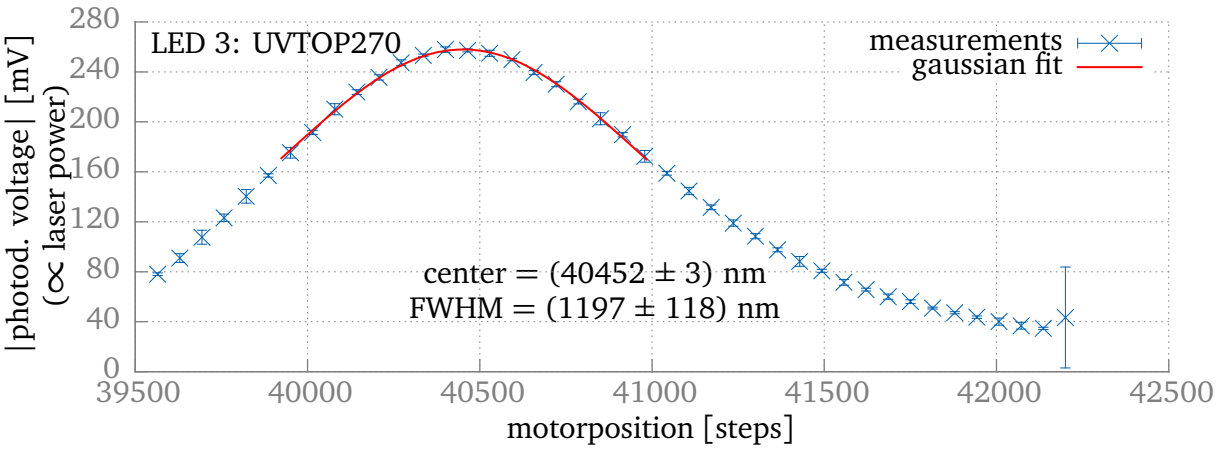

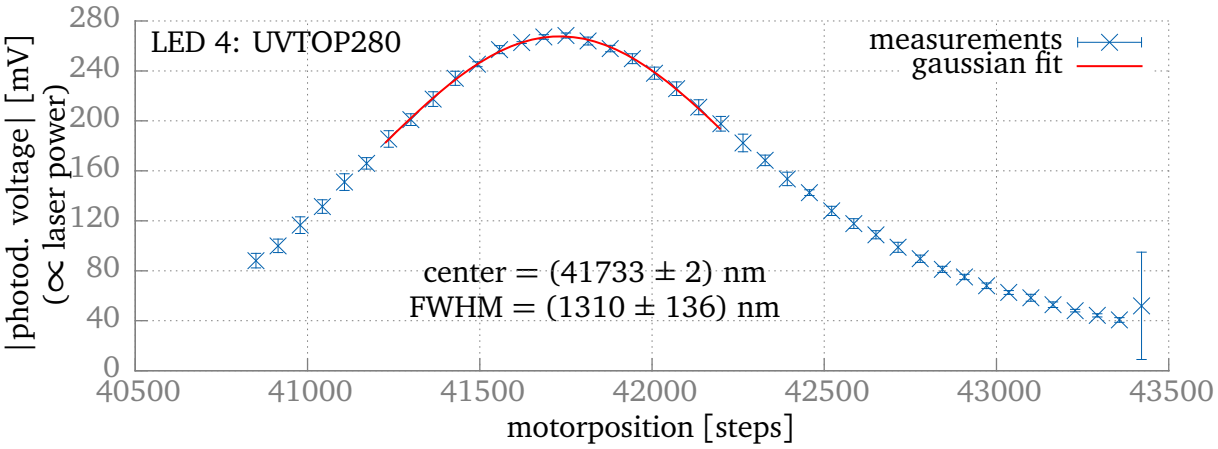

Figure 22: Measurement curves for the calibration of LED 2,3,4.

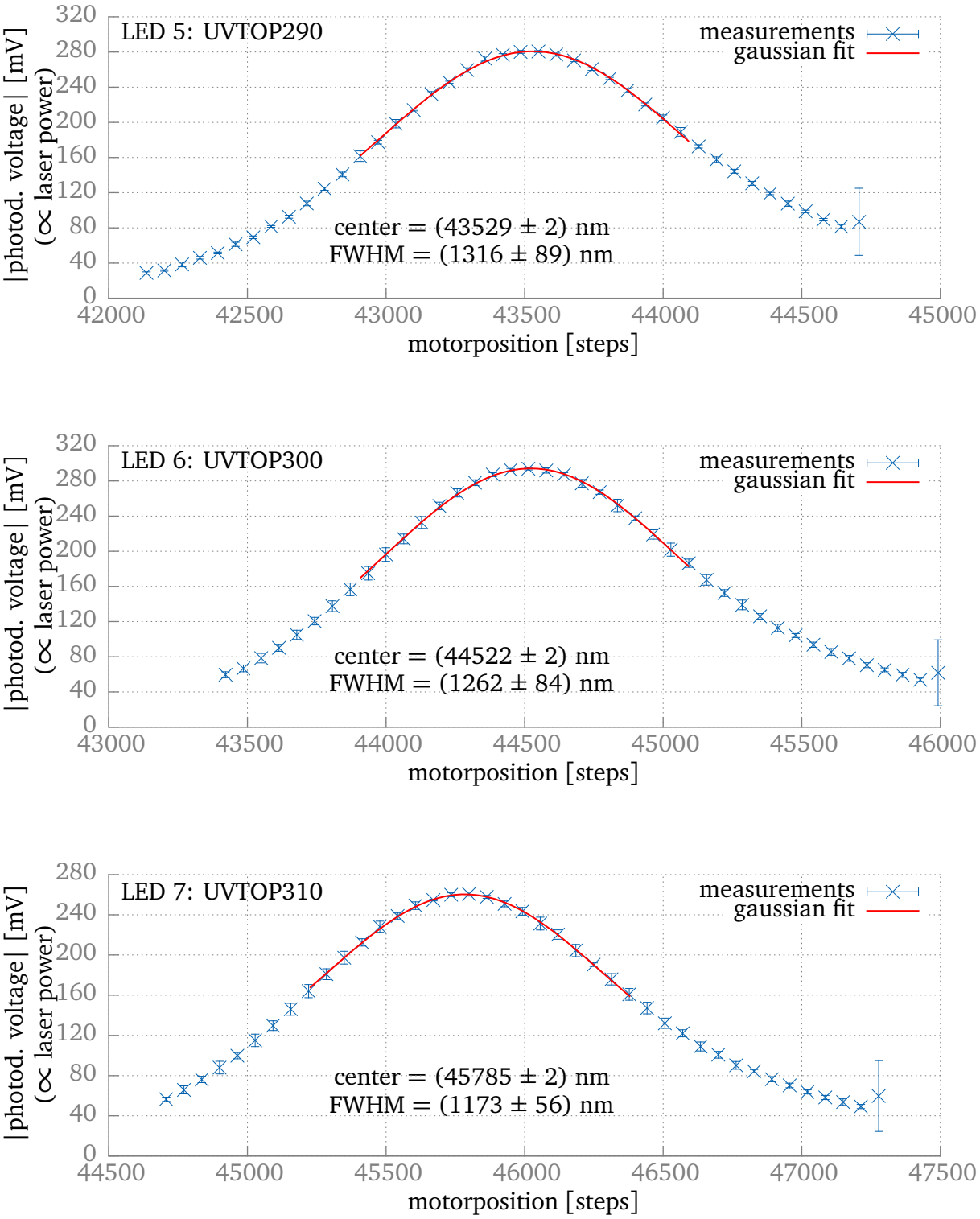

Figure 23: Measurement curves for the calibration of LED 5,6,7.

References

[Beh12] Jan Behrens: *Simulations of stored electrons in the Penning trap between the KATRIN spectrometers*, Diploma thesis, Institut für Kernphysik, Westfälische Wilhelms-Universität Münster, 2012.

[Beh14] Jan Behrens, personal communication.

[COD10] 2010 CODATA recommended values, <http://physics.nist.gov/cgi-bin/cuu/Value?hev>, [18.06.2014].

[CRC62] "Electron Work Function of the Elements" in Robert C. Weast, (Ed.): *CRC Handbook of Chemistry and Physics, 62th edition*, CRC Press, Boca Raton, FL, 1981. [13]

[HoH10] Horiba: *H10, H20 & DH10 - Compact Monochromators User Manual*.

[Hug08] K. Hugenberg, Diploma thesis, Institut für Kernphysik, Westfälische Wilhelms-Universität Münster, 2008

[IMP11] Institut für Materialphysik der WWU Münster: *Eigenschaften der Solarzelle*, 2011.

[KIT13] KIT webpage <http://www.katrin.kit.edu/>, [03.04.13].

[Pot13] Alexander Potthoff: *Aufbau einer durchstimmbaren UV-Lichtquelle für das KATRIN-Experiment*, Bachelor thesis, Institut für Kernphysik, Westfälische Wilhelms-Universität Münster, 2013.

[Pos11] Daniel Winzen, Volker Hannen, Hans-Werner Ortjohann, Michael Zacher, Christian Weinheimer: *Design of a pulsed angular selective electron gun for the Katrin main spectrometer*, poster, 2011.

[Rep14] Jan Behrens: *Report on the e-gun test measurements at the monitor spectrometer*, 2014, in preperation.

[UVT14] Roithner Lasertechnik GmbH webpage, <http://www.roithner-laser.com/led_deepuv.html#uvtop>

[Wik14] Wikipedia, The Free Encyclopedia, <http://en.wikipedia.org/wiki/Neutral_density_filter>, [14.07.2014]

[Win14] Daniel Winzen: *Development of an angular selective electron gun for the KATRIN main spectrometer*, Diploma thesis, Institut für Kernphysik, Westfälische Wilhelms-Universität Münster, 2014, to be published.

[Zac13] Michael Zacher: *Electron gun tests and characteristics*, presentation, 2013.

[Zac14] Michael Zacher, personal communication.

[13] In later versions I had on hand, only the work functions for single crystals are listed. Since we do not have a single crystal, an older version is quoted.

Danksagung

Ich danke Patrick, weil er ’ne verdammt geile Schnitte ist!

Plagiatserklärung

Hiermit versichere ich, dass die vorliegende Bachelorarbeit mit dem Titel “Characterisation of a photocathode for a monoenergetic electron source for the KATRIN experiment” selbstständig verfasst worden ist, dass keine anderen Quellen und Hilfsmittel als die angegebenen benutzt worden sind und dass die Stellen der Arbeit, die anderen Werken - auch elektronischen Medien - dem Wortlaut oder Sinn nach entnommenen wurden, auf jeden Fall unter Angabe der Quelle als Entlehnung kenntlich gemacht worden sind.

Ich erkläre mich mit einem Abgleich der Arbeit mit anderen Texten zwecks Auffindung von Übereinstimmungen sowie mit einer zu diesem Zweck vorzunehmenden Speicherung der Arbeit in eine Datenbank einverstanden.

Zudem versichere ich, dass ich die vorliegende Arbeit zum oben genannten Thema nicht bereits an anderer Stelle eingereicht habe.

_____

(Datum, Unterschrift)